

**Geochemical Investigation Into Holocene
Palaeoenvironmental Change Along The Southern Cape Coast,
South Africa**



WITS
UNIVERSITY

MSc Dissertation of Viwe Dyubele, 1439295

Supervisors:

Prof Marc Humphries

Dr Lynne Quick

School of Chemistry, Science Faculty

University of the Witwatersrand

Private Bag 3,

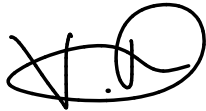
WITS, 2050

South Africa

Declaration

I, Viwe Dyubele, declare that this dissertation is my own unaided work, except where acknowledged and referenced. This dissertation is submitted following the requirements for the degree of Master of Science at the University of the Witwatersrand, Johannesburg. I have not submitted this work for examination at any other university.

Signature:

A handwritten signature in black ink, appearing to be 'Viwe Dyubele', written over a horizontal line.

Date: 08/06/2023

Student Name: Viwe Dyubele

Abstract

Climatic conditions across southern Africa are affected by the complex interaction of different atmospheric and oceanic circulation systems, the understanding of which is important to predicting future climate change. Palaeoenvironmental reconstruction is an essential tool to understand long-term environmental change and the response of ecosystems to such changes. This study examines the geochemical composition of a sediment core (WR1-1) extracted from a freshwater wetland located near Plettenberg Bay on the southern Cape coast. The wetland is located ~4 m above present sea level and positioned ~500 m from the modern coast. Situated within the year-round rainfall zone, the site is influenced by tropical easterly flow and the southern westerlies. Elemental and stable isotope geochemistry are used to reconstruct the palaeoenvironmental change at the site over the last ~8000 cal yr BP. Variations in $\text{CaO}/\text{Al}_2\text{O}_3$, $\text{Sr}/\text{Al}_2\text{O}_3$ and $\delta^{13}\text{C}$ indicate that marine conditions dominated from 7300 to 6400 cal yr BP. Marine influence at the site decreased dramatically from ~6300 cal yr BP, as the system transitioned to a freshwater back-barrier wetland. Enrichments in $\text{SiO}_2/\text{Al}_2\text{O}_3$ and $\text{Zr}/\text{Al}_2\text{O}_3$ track changes in depositional energy and suggest that the period 3800 – 3200 cal yr BP was associated with increased aeolian activity. This is interpreted to reflect increased aridity and is consistent with geochemical and pollen records from nearby sites at Eilandvlei and Voëlvlei. This suggests that a shift to more arid conditions during this time was a broad feature of the climate in the year-round rainfall zone of South Africa. The timing of this event corresponds with a marked decrease in Antarctic sea ice and pronounced aridity along the east coast of South Africa, suggesting that mid to late Holocene aridity in the YRZ was likely driven by declines in moisture from both westerly and easterly wind systems.

Acknowledgements

I would like to extend my gratitude to my supervisors Prof Marc Humphries and Dr Lynne Quick for the continuous guidance and support throughout my MSc journey, without their feedbacks and constructive input me I would have not made it thus far.

I would also like to thank the Tritisano Trust which I obtained through the Development and fundraising Office (DFO) of the University of the Witwatersrand and the Wits Hardship fund for providing funding towards my MSc degree.

I am grateful for the intentional support and constant motivation that I have gotten from my Mgoqi family through the years. My Dyubele family this is the first of many and hopefully more to come, thank for always encouraging me and believing in me.

The past two years have not been easy as I lost my grandmother SVN Mgoqi who raised me up. I would like to thank Chazani Gumede for inspiring me to always keep at it and always continue to work hard. My best friend Lubabalo Sawuli who has always been by my side throughout my university journey and all my other mates who have supported me.

Even nature has its own preserved narrative and what a beautiful journey it has been studying and interpreting it using its preserved geochemical information. This MSc degree is dedicated to the younger version of self that has always been intrigued by the beauty nature of her village Emazimeni. I thank God for He has been the source of everything throughout my life and my ancestors, oKhumalo, Amazima, oMgcina, oMgqithi, kude kwalapha bantu abadala uMdali enam, IViwe Imithandazo.

Table of contents

Declaration	2
Abstract	3
Acknowledgements	4
List of figures	7
List of tables	9
Chapter 1: Introduction	10
1.1 Background.....	10
Chapter 2: Literature Review	13
2.1 Modern regional climate.....	13
2.2 Holocene environmental changes	15
2.3 Sedimentary cores as archives of palaeoenvironmental information	17
2.4 Inorganic geochemistry proxies	18
2.5 Organic geochemistry proxies	19
Chapter 3: Regional setting	22
3.1 Regional climate	22
3.2 Regional Geology and Vegetation	23
Chapter 4: Methods and materials	25
4.1 Field work.....	25
4.2 Sediment dating and age modelling.....	26
4.3 Elemental analysis.....	26
4.4 Mineralogy	26
4.5. Stable isotope analysis.....	26
Chapter 5: Results	27
5.1 Core description and chronology	27
5.2 Elemental composition.....	30
5.3 Mineralogy.....	32
5.4 Chemical ratios	33

5.5	Stable isotope chemistry	34
Chapter 6: Discussion.....		36
6.1	Introduction.....	36
6.2	Proxy interpretation.....	36
6.3	Regional palaeoenvironmental comparison	40
6.4	Climatic drivers.....	44
Chapter 7: Conclusions.....		46
References		47
Appendix		53

List of figures

Figure 1.1 A) Map showing the location of the study site relative to other sites mentioned in the thesis. B) Zoomed in image of Whale Rock wetland.....	13
Figure 2.1 Map of southern Africa showing seasonality of rainfall and sharp climatic gradients that result in three distinct rainfall zones; winter (WRZ), year-round (YRZ) and summer (SRZ) rainfall zones. Major atmospheric and oceanic circulation systems and position of convergence zones (Inter-Tropical Convergence Zone (ITCZ), the Congo Air Boundary (CAB)) are also indicated (Chevalier and Chase, 2016), and B) Map showing the location of the study site relative to other sites mentioned in the thesis.....	16
Figure 2.2 Reconstructed sea-level change in South Africa over the last 9000 years based on the dating of marine shells and beach rock indicators (Ramsay, 1995; Compton, 2001).....	19
Figure 2.3 Relationship between $\delta^{13}\text{C}$ and C/N ratio (Lamb <i>et al.</i> , 2006).....	23
Figure 3.1 Map of southern Africa showing variation in mean annual precipitation and the present extent of the three major rainfall zones that characterise rainfall variability in the region; winter (WRZ), year-round (YRZ) and summer (SRZ) rainfall zones. The location of Whale Rock wetland near Plettenberg Bay is indicated by the red star.....	25
Figure 3.2 Graph showing month rainfall and temperature data recorded at Plettenberg Bay over the last thirty years. The mean daily maximum (solid red line), mean daily minimum (solid blue line), precipitation (blue bars) and cold nights and hot days (dashed blue and red lines).....	26
Figure 3.3 A) Geographic location of the study area, and B) Vegetation distribution of the southwestern Cape. Data source: South African National Land-Cover (2018).....	27
Figure 4.1 A) Location of the Whale Rock wetland situated near Plettenberg Bay along the southern Cape Coast, B) Google Earth image of Whale Rock Wetland showing the location of core WR1-1, and C) oblique photograph of the wetland showing the location of the coring site.....	28
Figure 5.1 Core section photographs of WR-1-1 showing variations in stratigraphy.....	30
Figure 5.2 Bayesian age-depth model of WR1-1.....	32
Figure 5.3 Downcore variations in LOI, SiO_2 , Al_2O_3 , K_2O , CaO and S through core WR-1-1. All XRF data are provided in Appendix 1.....	34

Figure 5.4 Relationship between selected major chemical components of sediments from WR1-1	35
Figure 5.5 X-ray diffraction (XRD) patterns and identified mineral phases for two samples: A) 219 – 225 cm (~7400 cal yr BP) and B) 161 – 165 cm (~6800 cal yr BP).....	36
Figure 5.6 Variation in chemical ratio indicators through core WR1-1.....	37
Figure 5.7 Downcore variation in C_{org}/N , $\delta^{13}C$ (‰) and $\delta^{15}N$ (‰) through core WR1-1.....	38
Figure 6.1 Comparison between marine influence geochemical indicators at Whale Rock (WR1- 1) with reconstructed variations in sea level along the southern Cape coast (Cooper et al., 2018) and sea surface temperatures (SST) from Nelson Bay Cave (Cohen and Tyson, 1995).....	40
Figure 6.2 Plot of $\delta^{13}C$ (‰) against C_{org}/N ratio for WR1-1 core samples. Standard ranges for organic inputs to coastal environments are indicated according to Meyers (1994). Samples associated with the sea level highstand shown in red.....	41
Figure 6.3 Comparison between key environmental proxies at Whale Rock. Macrocharcoal concentrations from Ntsondwa (2021). Grey shading indicates period of the record dominated by marine influence.....	43
Figure 6.4 Comparison of marine influence proxies from A) Whale Rock wetland (this study), B) Voëlvlei (Strobel et al., 2021), and C) Eilandvlei (Wündsche et al., 2018). Grey shading indicates period dominated by marine influence.....	44
Figure 6.5 Comparison of aridity proxies from A) Whale Rock wetland (this study), B) Eilandvlei (Wündsche et al., 2018) C) Voëlvlei (Strobel et al., 2021), and D) Eilandvlei (Wündsche et al., 2018). Grey shading indicates period dominated by marine influence.....	46
Figure 6.6 Comparison of aridity indicator data (Zr/Al_2O_3) from Whale Rock (A) with other palaeoclimate proxy records. B) Sea ice presence in the Southern Ocean (Nielsen et al., 2004), C) $\delta^{18}O$ temperature reconstruction from Cango Caves (Talma and Vogel, 1992), D) Elemental Ca/K record from Lake Muzi (Humphries et al., 2019), E) δD_{wax} record from the Limpopo River delta (Miller et al., 2020).....	48

List of tables

Table 5.1 Stratigraphic description of core WR-1-1.....	31
Table 5.2 Radiocarbon ages and calibration data for core WR1-1.....	32

Chapter 1: Introduction

1.1. Background

Climatic conditions across southern Africa are affected by the complex interaction of different atmospheric and oceanic circulation systems. Understanding the complexities and associated drivers behind climate variability in the region is important to predicting the nature of future climate variability and how ecosystems may respond to such change. Palaeoenvironmental reconstruction is an essential tool to understand long-term environmental change. This is particularly pertinent to the southern African region where existing records are scarce and future climate change rates are predicted to be high (Nangombe et al., 2018; Naumann et al., 2018).

Climate in the region is highly sensitive and influenced by both temperate and tropical circulation systems (Quick et al., 2018). Available palaeoenvironmental records from the regional indicate that climate has likely been highly dynamic over time, with tropical and temperate systems having responded to changing global boundary conditions (Chase and Meadows, 2007; Chase et al., 2017; Quick et al., 2018). Although recent work along the southern Cape coast (e.g., Kirsten et al. 2018; Wündsche et al. 2018; Strobel et al. 2021; Quick et al., 2021) has contributed greatly to unravelling the complex nature of these climatic interactions and associated environmental responses, our understanding of finer-scale spatial variability in environmental response, particularly over the Holocene, remains less well-constrained.

Wetland and lake deposits offer valuable prospects for reconstructing past environmental change. The geochemical signatures they preserve over time record variations that have occurred both within the waterbody itself (*in-situ*) and from the surrounding catchment area (*ex-situ*), and have proved to be extremely useful in reconstructing environmental and climatic changes in southern Africa (Humphries et al., 2021). Several coastal lakes in the southern Cape have been investigated from a geochemical perspective (e.g., Eilandvlei, Groenvlei and Voelvlei; Fig. 1.1) and provided detailed Holocene environmental information that has assisted in unravelling past climate dynamics in the region (Wündsche et al., 2016; Wündsche et al., 2018; Strobel et al., 2021).

1.2 Project aim and objectives

This study examines the geochemical composition of an approximately 302 cm long sediment core extracted from the freshwater coastal Whale Rock wetland located near Plettenberg Bay on the southern Cape coast (Fig. 1.1A). The wetland site has not previously been studied from a palaeoenvironmental perspective. Situated within the year-round rainfall zone, the site is influenced by tropical easterly flow and the southern westerlies, and offers the potential for investigating changes in the strength and position of these large-scale atmospheric circulation systems.



Figure 1.1 A) Map showing the location of the study site relative to other sites mentioned in the thesis, and B) Zoomed in image of Whale Rock wetland

Whale Rock wetland, also known as Robberg Vlei (-34.090035 S, 23.367352 E), is a natural freshwater wetland located in Plettenberg Bay on the southern Cape coast of South Africa (Fig. 1.1B). The wetland occupies an inter-dunal depression and covers an area of approximately 2.6 km². The system is isolated from the ocean behind a 20 m high coastal dune and surrounded largely by residential development. No hydrological studies have been conducted, but it is assumed the wetland is supplied mainly by groundwater and direct rainfall. The wetland vegetation dominated by dense stands of *Phragmites*.

The overarching aim was to reconstruct Holocene palaeoenvironments at the site using geochemical techniques and compare these records with other sites to better understand changes in the broader southern Cape region.

The following objectives were identified:

- Examine changes in sediment deposition and source using inorganic elemental analysis and stable isotopes (¹³C, ¹⁵N).
- Use geochemical changes recorded in the sedimentary record to reconstruct palaeoenvironments at Whale Rock.
- Compare palaeoenvironmental information revealed by the analysis of sediments from Whale Rock to other palaeo-records from the southern Cape region.

Chapter 2: Literature Review

2.1. Modern regional climate

Southern Africa is positioned at a boundary interface between temperate and subtropical systems and is thus highly sensitive to multiple forcing mechanisms that result in high degree of climatic variability (Hahn et al., 2016; Quick et al., 2016; Chevalier and Chase, 2016). Climate in the region is influenced by shifts of the Intertropical Convergence Zone (ITCZ), Southern Hemisphere Westerlies (SHW) and position of subtropical cyclones (Chase and Meadows, 2007). The relative dominance of these temperate and tropical systems is reflected by strong seasonality in rainfall across the region, which produces three distinct rainfall regimes (Chase and Meadows; Fig. 2.1). The central and eastern parts of the country receive most rainfall (> 66%) from subtropical moisture-bearing atmospheric circulation systems during the austral summer (Summer Rainfall Zone, SRZ). In contrast, the southern and western coasts of South Africa receive most rainfall (> 66%) from temperate SHW as cut-offs and ridging anticyclones during the austral winter (Winter Rainfall Zone, WRZ). An intermediate area between the SRZ and WRZ receives rainfall from both temperate and subtropical systems throughout the year (Year-round Rainfall Zone, YRZ).

The southern Cape coast experiences dominantly year-round rainfall and has climate described as temperate oceanic (Du Plessis et al., 2020). Rainfall averages 800 to 1000 mm with increased rainfall from March to April and September to October (Chevalier and Chase, 2016; Du Plessis et al., 2020). Mean annual temperatures in the region average between 15 and 18 °C with the central region (Cape Agulhas to George) experiencing slightly higher temperatures compared to the eastern afrotemperate section (Du Plessis et al., 2020).

The southern Cape coast is influenced by Berg winds, which occur mostly during winter and blow in a north-westerly to north-easterly direction from the drier interior of the country (Du Plessis et al., 2020). These winds are characteristically hot and dry and produce changes in temperature and moisture availability across the southern Cape coast (Du Plessis et al., 2020). Climate in the region is also strongly influenced by the Agulhas Current which introduces warm

water along the eastern Agulhas Bank and provides an important source of moisture (Tyson and Preston-Whyte 2000; Du Plessis et al., 2020).

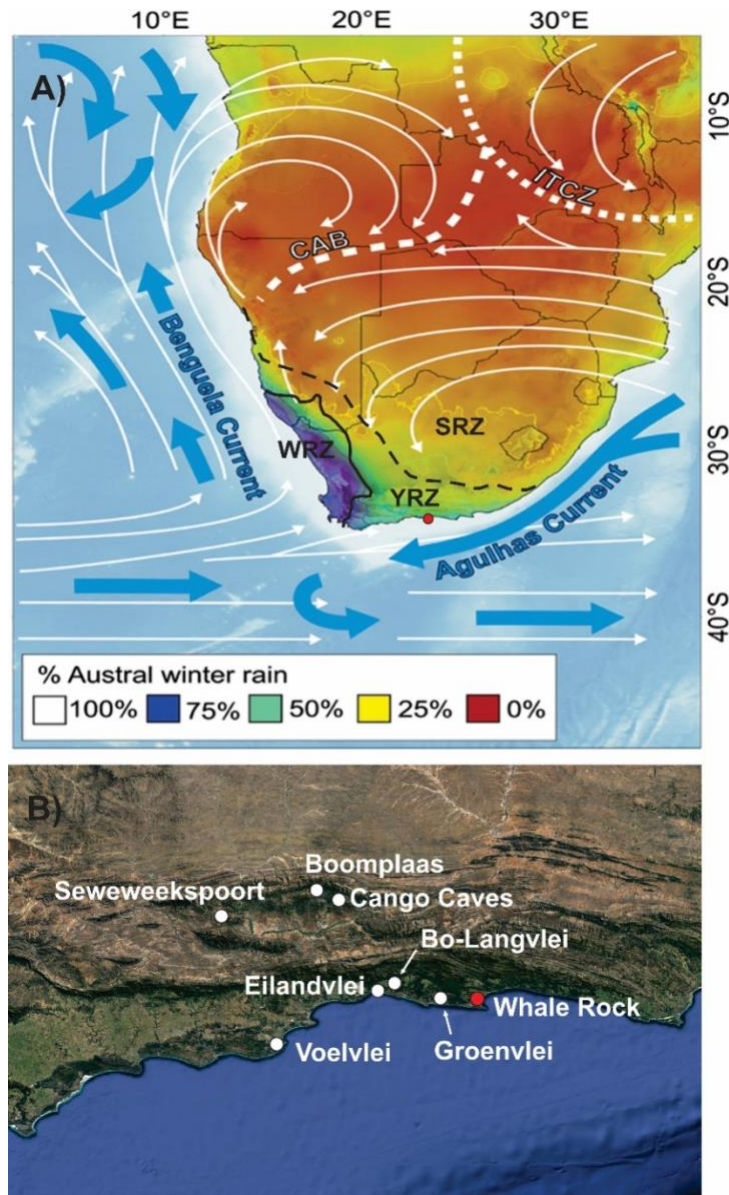


Figure 2.1 A) Map of southern Africa showing seasonality of rainfall and sharp climatic gradients that result in three distinct rainfall zones; winter (WRZ), year-round (YRZ) and summer (SRZ) rainfall zones. Major atmospheric and oceanic circulation systems and position of convergence zones (Inter-Tropical Convergence Zone (ITCZ), the Congo Air Boundary (CAB)) are also indicated (Chevalier and Chase, 2016). The location of Whale Rock wetland near Plettenberg Bay is indicated by the red dot, and B) Map showing the location of the study site relative to other sites mentioned in the thesis.

2.2 Holocene environmental changes

Climatic projections suggest an increase in the frequency and magnitude of extreme climatic events in southern Africa (Pohl et al., 2017; Nangombe et al., 2018) and the generation of detailed palaeoenvironmental data from critical regions are essential. Palaeoreconstructions are useful for the understanding climatic variability over longer periods of time and provide context for evaluating ecosystem response to future climate change (Du Plessis et al., 2020; Humphries, 2021).

The South African coastline has been markedly influenced by Quaternary sea-level changes. A significant portion of the Agulhas Bank was submerged by increasing sea level following the termination of Last Glacial Maximum (LGM) ~20,000 years ago (Compton, 2001; Cawthra et al., 2020). Warmer global temperatures and accelerated deglaciation led to rapid sea level rise along the South African coastline in the order of 8 mm/yr, before reaching present day levels ~7000 cal yr BP (Ramsay, 1995). Sediments stored in the shoreface, migrated inland with sea-level rise forming transgressive barriers that led to the development of most modern estuaries and lagoons, including those along the southern Cape coast. Ramsay (1995) suggests that sea level reached a highstand at 3.5 m ~5300 cal yr BP. Many studies have recorded marine transgressions during the mid-Holocene, although uncertainties remain with respect to the timing and magnitude of these events.

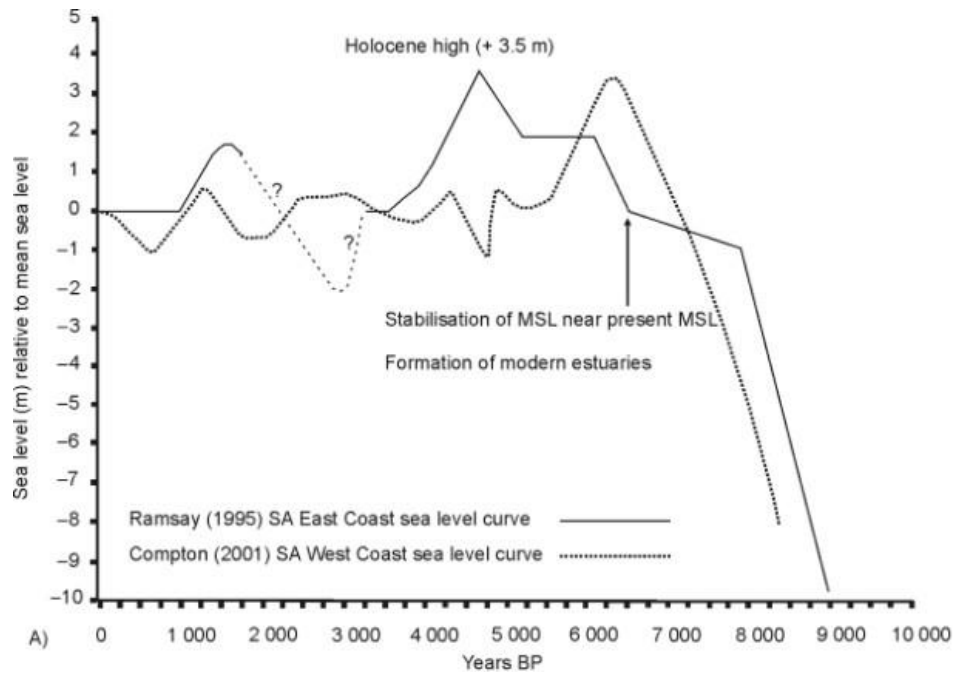


Figure 2.2 Reconstructed sea-level change in South Africa over the last 9000 years based on the dating of marine shells and beach rock indicators (Ramsay, 1995; Compton, 2001).

The Holocene (dating from ~12,000 cal yr BP) is the most recent stratigraphic epoch (Cohen et al., 2020). This period of earth’s history has been associated with marked and often rapid fluctuations in climate and sea level globally. Several studies have highlighted the dynamic nature of the southern Cape coast in response to Holocene changes in climate and sea level. This has included evidence from stalagmites at Cango Caves (Talma and Vogel, 1992), hyrax middens at Seweweekspoort (Chase et al., 2013, Chase et al 2017) and coastal lakes Groenvlei (Wündsche et al., 2016), Eilandvlei (Kirsten et al., 2018; Quick et al., 2018; Wündsche et al., 2018) and Bo-Langvlei (Du Plessis et al., 2020).

Stable isotope records from Seweweekspoort suggest that the start of the Holocene (11800 to 10700 cal yr BP) was characterised by a distinct humid episode (Chase et al., 2013). This was associated with establishment of elevated interglacial temperatures and a sharp decline in sea-ice extent (Chase et al., 2017). Following this, microfaunal and pollen data from Boomplaas Cave suggest that cooler conditions prevailed 10100 – 8900 cal yr BP (Faith et al., 2019). Pollen, microcharcoal and geochemical data from Eilandvlei indicates that arid and cool conditions prevailed between ~8900 and 8000 cal yr BP (Quick et al., 2018; Wündsche et al., 2018),

suggesting a weakening in the influence of the westerlies during this time.

Geochemical (Fe, Si/Al) and grainsize data from Eilandvlei point to increased rainfall and river discharge between ~7900 and 6400 cal yr BP (Wündsche et al., 2018). A generally wetter climate over this time is supported by an expansion in afrotemperate forest from 8000 to 4700 cal yr BP (Quick et al., 2018) and is consistent with increased humidity between 7000 and 5000 cal yr BP indicated by isotope analysis of hyrax middens from Seweweekspoort (Chase et al., 2013). This was followed by cool and arid conditions 6400 – 3000 cal yr BP as indicated by increased grainsize and enhanced aeolian deposition at Eilandvlei (Wündsche et al., 2018). Isotope analysis of stalagmites at Cango Caves suggest temperatures 4500 – 3000 cal yr BP were 1-2 °C lower compared to the present (Talma and Vogel, 1992). Mineralogical, isotopic and geochemical analyses from Groenvlei support this and indicate generally dry conditions between 4210 and 2710 cal yr BP (Wündsche et al., 2016). Conditions from 3000 cal yr BP to present were characterised by a steady increase in moisture as indicated by the long-term increase in forest taxa at Eilandvlei (Quick et al., 2018; Wündsche et al., 2018).

High-resolution fossil pollen and microcharcoal records from Bo Langvlei spanning the past ~1300 years suggest the period 1000 – 700 cal yr BP was dry and slightly cooler than present (reduced levels of Afrotemperate forest pollen and increased percentages of Stoebe-type pollen). The Little Ice Age (LIA; 650 – 100 cal yr BP) was identified as a period of cool, dry conditions, associated with the expansion of drought-sensitive forest taxa such as *Podocarpus* (Du Plessis et al., 2020). In contrast, midden records from Seweweekspoort suggest wetter conditions during the LIA (Chase et al., 2013).

2.3 Sedimentary cores as archives of palaeoenvironmental information

Wetland and lake systems are sensitive to both climatic (e.g, rainfall and temperature) and catchment-scale environmental (e.g., vegetation cover and sediment supply) changes. The sediments trapped within these systems thus often preserve material of the area that provides useful palaeoenvironmental information (Du Plessis et al., 2020; Humphries et al., 2021 Meyers ,

2003). Lake and wetland sediments typically consist of organic and inorganic components that have different origins and offer potential proxies for interpreting past environments. Geochemical proxies can be used to investigate different environmental processes and when used together can provide significant palaeoenvironmental information to complement other proxy data (e.g., pollen) and enhance our ability to reconstruct past climate change.

The geochemical composition of sediments is largely controlled by chemical processes that take place during weathering, transport, and deposition (Humphries et al., 2021). Geochemical analysis of sediments can thus be used to understand the nature of these processes under varying climatic conditions (Francke et al., 2020). Palaeoenvironmental information may be derived from examining the chemistry of both the inorganic and organic component of sediments, each of which can provide unique insight into the depositional history of the site. An overview of the proxies used in this study is provided below.

2.4 Inorganic geochemistry proxies

Inorganic geochemical analysis provides information on the distribution and concentration of elements and radionuclides (Francke et al., 2020). The use of X-ray fluorescence (XRF) has become increasingly popular in palaeoclimate studies because it is multi-element and non-destructive, allowing the generation of high-resolution elemental records (Croudace et al., 2019). Elemental records obtained by XRF provide a variety of potential geological tracers that can offer unique insight into different climate-mediated sediment processes. This section provides a brief description of the geochemical proxies used in this study.

The analysis of geochemical data together with grain size size together is often used to reflect the changes in the depositional energy of the sedimentary material at the core site which can support palaeoenvironmental reconstructions. Aluminium (Al) is often used as a reference element in such cases as it is predominantly associated with aluminosilicates and typically not affected by redox or biological processes (Schropp et al., 1990). Heavy minerals together with grain size are often good indicators of depositional energy. Enrichment in Zr/Al and Si/Al thus indicates increases in depositional energy associated with changing climatic conditions (Humphries, 2020; Kylander et al., 2011). Similarly, Si/Al ratios can be used to identify periods of enhanced aeolian

influx, as it reflects the proportion of quartz to feldspars and other aluminosilicates. Thus, a high Si/Al ratio may be related to enhanced transport of sand-size material during drier periods (e.g., Wündsche et al., 2018).

Marine water is relatively enriched in certain chemical components, for example sulfates, calcium, strontium and sodium, compared to freshwater. The intrusion of marine water into coastal lakes and wetlands can thus be potentially traced by examining enrichments in these components (Riley and Chester, 2013; Schoepfer, 2013). For example, enrichment in S/Al was used to indicate periods of marine intrusion associated with sea-level rise on the east coast of South Africa (Higgs et al., 2017). Calcium carbonate is supersaturated in seawater and forms a key component of many marine organisms (e.g., mollusc shells). In certain situations, therefore, the presence of calcium minerals within coastal deposits can be used as a proxy to infer changes in the degree of marine influence (e.g., Wündsche et al., 2016, 2018). Other potential indicators of marine water intrusion include Sr, Na and Br (e.g., Strobel et al., 2021).

2.5 Organic geochemistry proxies

Organic matter present in wetland and coastal lake sediment is typically derived from two primary sources: 1) from the catchment and transported via run-off (allochthonous), and 2) produced in the lake/wetland through the process of photosynthesis (autochthonous) (Meyers, 2003). Organic geochemical analysis provides information on the quantity and composition of organic compounds present within sediments.

Information on the origin of sedimentary organic matter can be derived from stable isotope composition ($\delta^{13}\text{C}$ and $\delta^{15}\text{N}$) of the material. The $\delta^{13}\text{C}$ composition of terrestrial, freshwater, and marine plants is different as plants assimilate carbon from different sources. The photosynthetic pathways for terrestrial plants is either C_3 (shrubs and trees), C_4 (tropical grasses) or CAM (succulents), all of which have distinctively different ways of processing atmospheric carbon dioxide, resulting in different $\delta^{13}\text{C}$ signatures. C_3 vegetation is commonly found in the WRZ and includes fynbos, while C_4 grasses occur mostly in the SRZ (Stock et al., 2004).

Marine plants utilise dissolved inorganic carbon (from dissolved bicarbonate) and yield organic matter characterised by $\delta^{13}\text{C}$ signatures ranging between -16‰ to -25‰ (Lamb et al., 2006; Meyers, 1997). Freshwater aquatic plants utilise dissolved carbon dioxide, while terrestrial plants use the carbon dioxide from the atmosphere (Mackie et al., 2005). The $\delta^{13}\text{C}$ signature of the resulting organic matter from these two types of plants is indistinguishable from each and typically ranges from -21‰ to -32‰ (Lamb et al., 2006). However, the ratio of total organic carbon (TOC) to total nitrogen (TN) can be used to distinguish between terrestrial-derived plant organic matter and aquatic/marine plant organic matter (Meyers, 1994). Algae and bacteria have lower values of the TOC/TN ratio (between 4 – 10) due to higher nitrogen levels in aquatic plants, while terrestrial vegetation is characterised by higher TOC/TN values (above 20) (Lamb et al., 2006) (Figure 2.3). This distinction arises as result of aquatic plants enriched in proteins resulting in increased nitrogen levels whereas terrestrial plants are cellulose-rich and contain lignin.

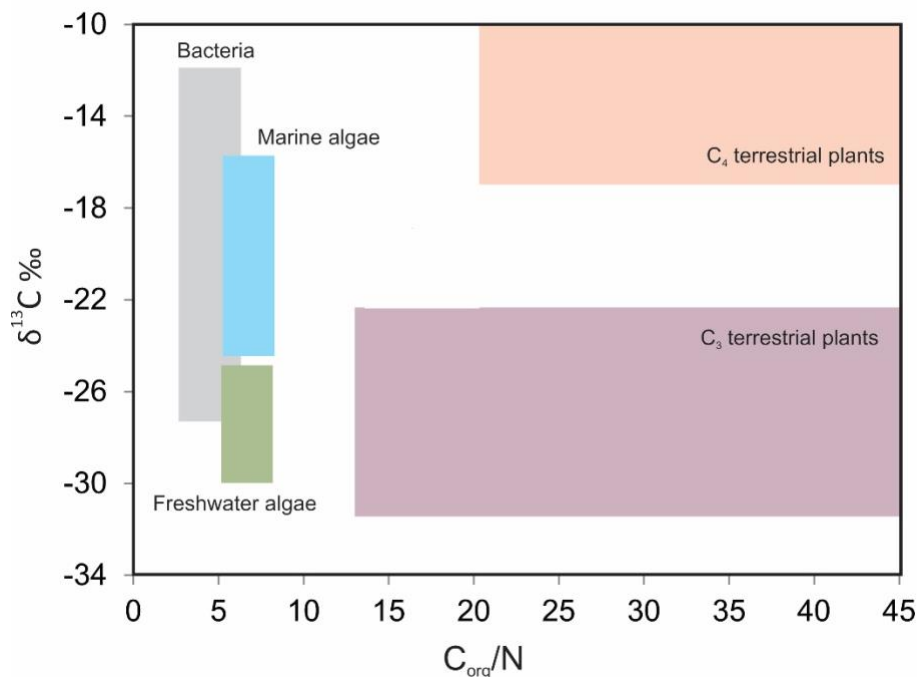


Figure 2.3 Relationship between $\delta^{13}\text{C}$ and C/N ratio (Lamb et al., 2006).

Nitrogen is a redox sensitive element, existing in different forms (N_2 , NO_3^- , NH_4^+) depending on conditions. Nitrogen is introduced to marine environments through nitrogen fixation (N_2) by cyanobacteria and phytoplankton, where it is reduced to NH_4^+ and assimilated with minimal fractionation, typically -2 to +1‰ (Wada et al., 1975). In the presence of oxygen, NH_4^+ undergoes oxidation to nitrate (NO_3^-), a process known as nitrification, which results in significant fractionation of up to +20‰. In the absence of oxygen, denitrification occurs and nitrates are partially reduced to N_2 and N_2O (Cartigny et al. 2018).

Chapter 3: Regional setting

3.1 Regional climate

Plettenberg Bay occurs in the YRZ (Fig. 3.1) and has a climate classified as cool and rain occurs throughout the year (Quick et al., 2013). October typically receives most rain with an average 48 mm with lowest rainfall occurring in January with an average 23 mm (Fig. 3.2). Maximum temperatures are reached between December and March (average 26-27 °C) while minimum temperatures occur between June and August (average 9-11 °C) (www.meteoblue.com). The southern Cape coast is dominated by strong south-westerly winds throughout the year, which frequently reach velocities in excess of 40 km/h (Hellström and Lubke, 1993). Secondary winds of lower frequency blow from the south-east, while easterly winds are infrequent.

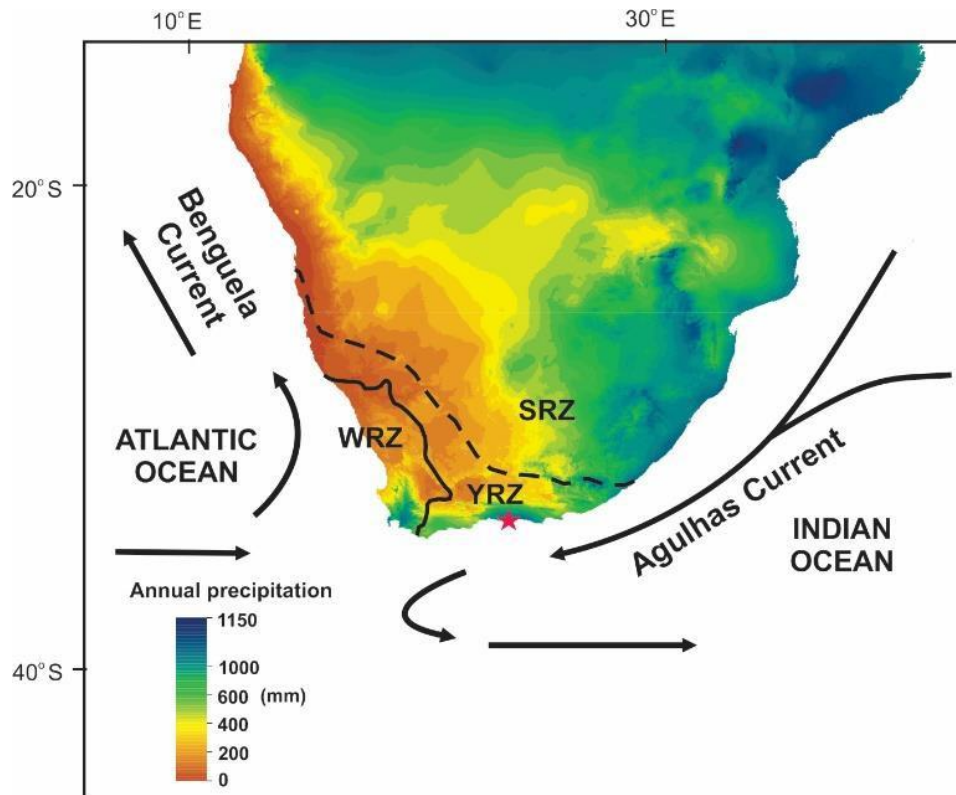


Figure 3.1 Map of southern Africa showing variation in mean annual precipitation and the present extent of the three major rainfall zones that characterise rainfall variability in the region; winter (WRZ), year-round (YRZ) and summer (SRZ) rainfall zones. The location of Whale Rock wetland near Plettenberg Bay is indicated by the red star.

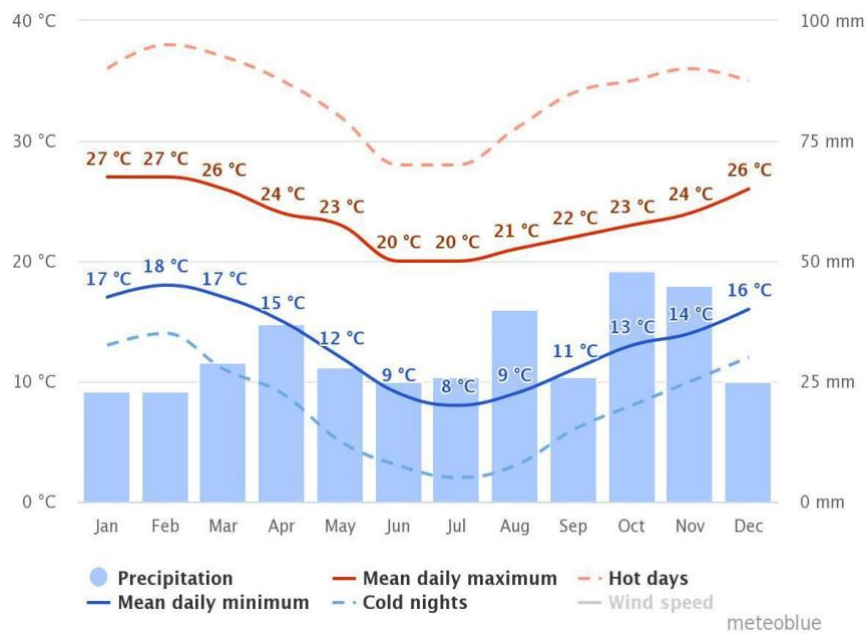


Figure 3.2 Graph showing month rainfall and temperature data recorded at Plettenberg Bay over the last thirty years. The mean daily maximum (solid red line), mean daily minimum (solid blue line), precipitation (blue bars) and cold nights and hot days (dashed blue and red lines) (www.meteoblue.com).

3.2 Regional Geology and Vegetation

Plettenberg Bay lies on a wave-dominated, microtidal coast. The coastline is dominated by the headland-bay system defined by the Robberg Peninsula (Fig. 3.3A). The peninsula is about 4 km long and rises up to ~140 m above sea level (Flemming and Martin, 2021). The wave climate is dominated by ocean swells propagating from the south-west. The tidal range in Plettenberg Bay reaches almost 2 m at spring tide (Schumann et al. 1982).

The onland bedrock geology is predominantly composed of sandstones and quartzites belonging to various formations of the Cape Supergroup (Carr et al., 2019). At Plettenberg Bay, these comprise of predominantly quartzitic sandstones of the Table Mountain Group. Deposits of the Uitenhage Group crop out at Robberg. Vegetation falls within the Fynbos Biome and comprises a mosaic of shrubs, grassland, and forest (Fig. 3.3B). All shrub and tree species are C₃, while grasses that occur in the region comprise both C₃ and C₄ species (Vogel et al., 1978). Terrestrial vegetation at Plettenberg Bay is classified as Garden Route Shale Fynbos and is dominated by ericaceous and

proteoid fynbos (Mucina and Rutherford, 2006). Knysna Sand Fynbos can be found on Robberg Peninsula.

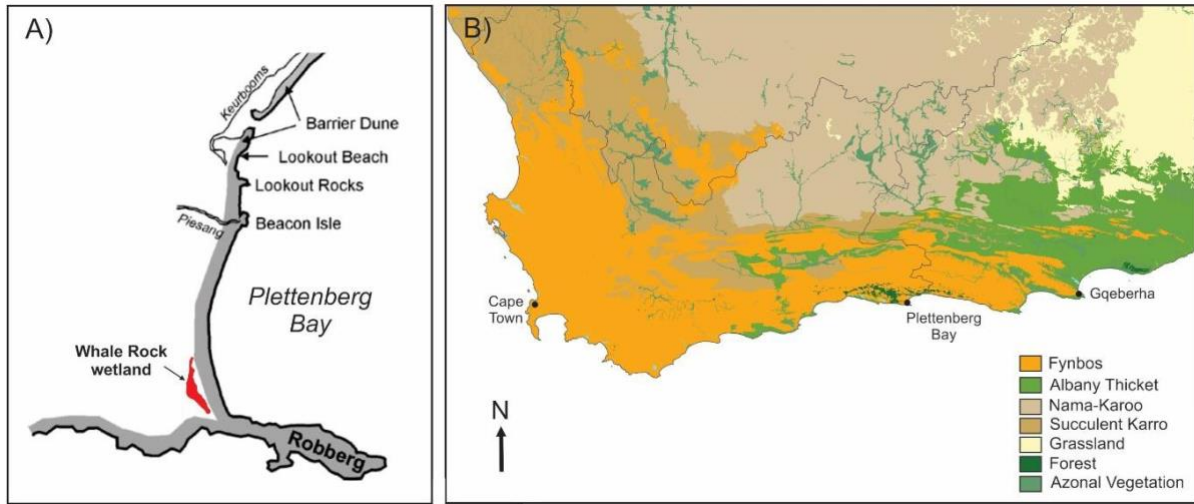


Figure 3.3 A) Geographic location of the study area, and B) Vegetation distribution of the south-western Cape. Data source: South African National Land-Cover (2018)

Chapter 4: Methods and materials

4.1. Field work

Sediment core WR-1-1 (34.090035 S; 23.367352 E) was retrieved from Whale Rock wetland at Plettenburg Bay on the southern coast of South Africa in October 2020 (Fig. 4.1). The WR-1-1 measures 302 cm and was collected using a Russian corer. Core sections were transferred into half-round 50 mm PVC tubes, wrapped in cling film, and transported to Nelson Mandela University where they were stored at 4 °C.



Figure 4.1 A) Location of the Whale Rock wetland situated near Plettenburg Bay along the southern Cape Coast, B) Google Earth image of Whale Rock Wetland showing the location of core WR1-1, and C) oblique photograph of the wetland showing the location of the coring site.

4.2 Sediment dating and age modelling

An age-depth model for WR-1-1 was constructed from seven radiocarbon ages. Bulk organic subsamples were dated at Queen's University, Belfast, using Accelerator Mass Spectrometry (AMS). Radiocarbon ages were calibrated to calendar years using the Southern Hemisphere atmospheric curve SHCal.13 (Hogg et al., 2013, Table 1) and an age–depth model was developed in R software package Bacon (v. 2.3.6) (Blaauw and Christen, 2011).

4.3 Elemental analysis

Subsamples for geochemical analysis were taken at 2 cm intervals. Sediments (n = 136) were dried at 105 °C and milled to homogenous powders. Organic matter was measured as a weight percentage by loss on ignition (LOI) at 550 °C for 4 hours. Combusted powders were then analysed for major element composition by X-ray fluorescence (XRF) at the University of the Witwatersrand (Bruker S2 Ranger). The instrument was calibrated against a range of local and USGS rock standards and measured concentrations were typically within 10% of accepted values. Internal precision was < 2% for all elements based on the repeated analysis of USGS rock standards GSP2 and AVG2.

4.4 Mineralogy

The mineralogy of selected sediment samples (based on their elemental composition) was investigated by X-ray diffraction (XRD). Dried powders were run using a Bruker D2 Phaser X-ray diffractometer (7 to 60° 2 θ) with monochromated CoK α radiation from 7° to 50° 2 θ .

4.5. Stable isotope analysis

A total of 65 samples were selected for stable isotope ($\delta^{13}\text{C}$ and $\delta^{15}\text{N}$) analysis based on the age-depth model. Samples were treated with 10% HCl to remove carbonate and dried at 60 °C before being milled to a fine powder. Isotope analyses were conducted at the University of Cape Town using isotope ratio mass spectrometry (IRMS).

Chapter 5: Results

5.1. Core description and chronology

The upper ~60 cm of the core consisted of dark brown organic-rich mud containing large quantities of plant material. Underlying sediments from 60 – 196 cm were composed of grey-brown to yellowish-brown peat with the occasional presence of shell fragments. A distinct change at 196 cm marked a transition to brown clayey mud, characterised by mottles and shell fragments. Thin reddish striations were observed between 230 and 240 cm. The basal unit (302 – 280 cm) comprised coarse light grey to white sand, which graded down into medium grey-brown sand with fine shell fragments.



Figure 5.1 Core section photographs of WR-1-1 showing variations in stratigraphy

Table 5.1 Stratigraphic description of core WR-1-1

Unit	Depth interval (cm)	Description	Munsell colour
1	0 – 6	Root mat layer, medium brown organic-rich muddy sediments with a lot of fibrous plant material	5Y 4/4
2	6 – 58	Very dark brown, very organic-rich peat with large quantities of plant material	5GY 1/2
3	58 – 122	Medium grey-brown peat with plant material, shells and shell fragments, mottles of top unit within this unit, less compacted than previous unit	5GY 1/2
4	122 – 196	Lighter yellowish-brown sediments, moderate organic content with plant material, shell fragments, dark mottles	7.5Y 4/3 Mottles: 10Y 2/2
5	196 – 202	Medium brown clayey mud with mottles, shells fragments, large pieces of plant matter, less organic than previous unit	5Y 6/6 (lighter) 5Y 3/4 (darker)
6	202 – 280	Dark brown, organic-rich peat, no shell fragments, less identifiable plant matter, thin reddish striations from ~230 - 240 cm	5Y 1/1 Striations: 5YR 3/6
7	280 – 302	Medium grey- brown sand grading down into coarser light grey with white grains, sand, fine shell fragments, some dark brown organic-rich mottles interspersed sparsely through unit	7.5Y 4/2

The seven radiocarbon dates obtained for WR-1-1 yielded a coherent age-depth model, indicating a basal age of ~8500 cal yr BP for the 302 cm profile (Table 5.2; Fig. 5.2). A sample from 13 cm produced a result of $1.08 \pm 0.19\%$ pMC, indicating that sediment at this depth contained modern (post-1950) carbon. All age determinations are stratigraphically consistent but suggest a marked change in sedimentation rate at ~6500 cal yr BP. Sedimentation rates from 8500 – 6500 cal yr BP average $\sim 0.11 \text{ cm yr}^{-1}$, but decrease to $\sim 0.02 \text{ cm yr}^{-1}$ from 6500 cal yr BP to present.

Table 5.2 Radiocarbon ages and calibration data for core WR1-1

Lab Code	Depth interval (cm)	^{14}C Age (yr)	Calibrated age (cal yr BP)
UBA-43908	13	Modern	
UBA-43147	47	2335 ± 24	2223
UBA-43155	63.5	2778 ± 25	2827
UBA-43156	89.5	4739 ± 47	5425
UBA-43909	120.5	5705 ± 25	6482
UBA-43148	181	6139 ± 23	6974
UBA-43910	271.5	7085 ± 26	7883

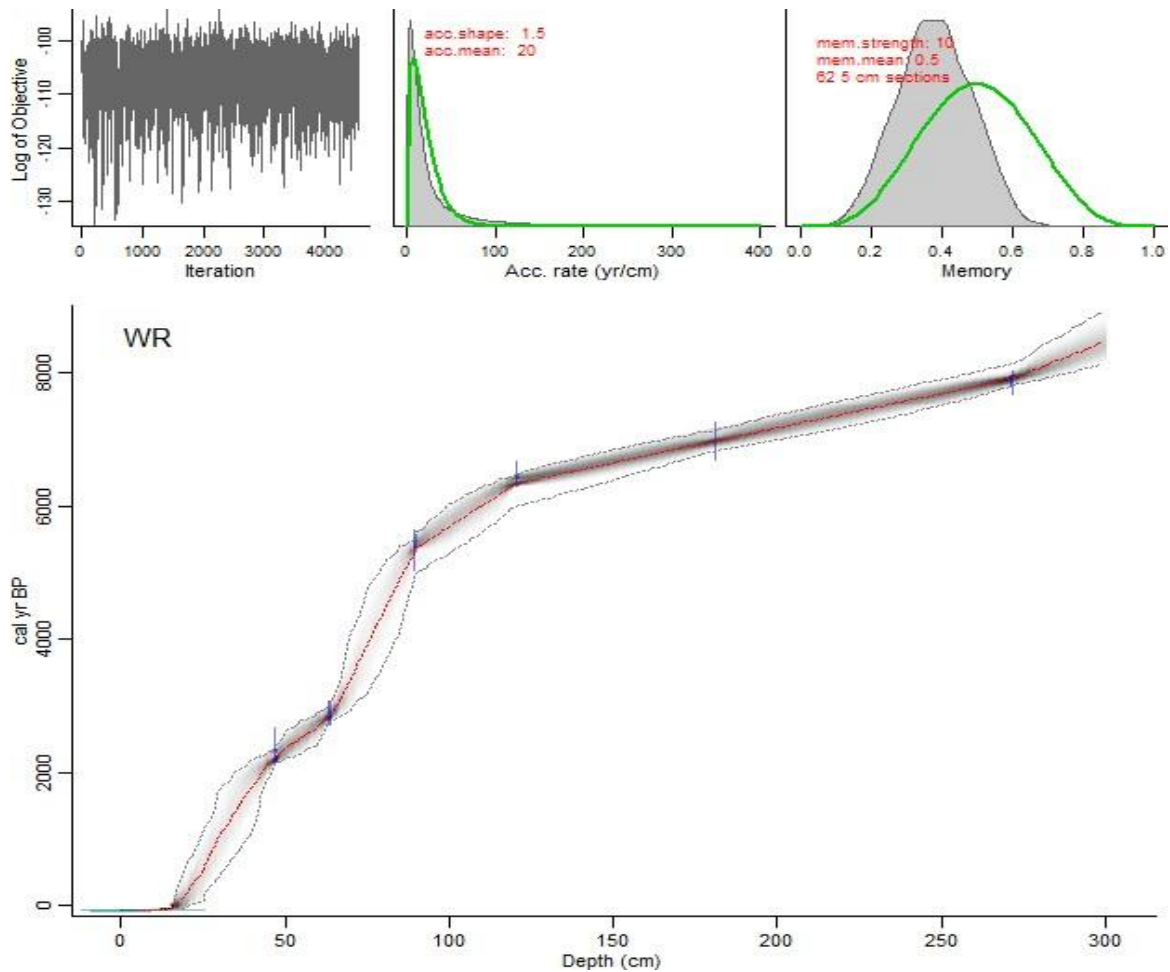


Figure 5.2 Bayesian age-depth model of WR1-1

5.2. Elemental composition

Measured LOI varied considerably downcore ranging between 1.3% and 93 % (Fig. 5.3A). The basal sand deposit (8350 – 8000 cal yr BP) is characterised by very low LOI (< 2%), but a sharp transition to a highly organic-rich material (LOI > 80%) occurs between ~8000 and 7200 cal yr BP. A distinct decrease in %LOI is observed between 7200 and 6400 cal yr BP, followed by markedly higher values between 6400 and 4500 cal yr BP. A gradual decrease in %LOI occurs 4500 – 3600 cal yr BP, with values remaining relatively constant (40 – 50%) from 3500 cal yr BP to present.

Concentrations of SiO₂ vary between 10% and 70% and are typically inversely related to %LOI (Fig. 5.3B). Highest SiO₂ contents (65 – 70%) were found at the base of the core (8350 – 7900 cal yr BP). Sediments from 7900 – 4500 cal yr BP contained much lower, although variable (averaging ~20%), SiO₂ contents. A sharp increase is observed between 6500 and 6320 cal yr BP. A gradual increase in %SiO₂ is observed from ~4500 to 3000 cal yr BP, with concentrations remaining relatively constant (50 – 60%) over the last 3000 years. A sharp decrease in %SiO₂, however, is observed between 2170 and 2060 cal yr BP.

Variations in %Al₂O₃ (Fig. 5.2C) and %K₂O (Fig. 5.2D) show similar downcore trends. Sediments from 8350 to 3250 cal yr BP generally contain relatively low concentrations of Al₂O₃ (< 5%) and K₂O (< 1%). Abundance in Al₂O₃ and K₂O increases markedly from ~3250 cal yr BP to present, with concentrations reaching up to 16.8% and 1.8%, respectively.

Marked variations in CaO (Fig. 5.2E) and S (Fig. 5.2F) concentrations are observed through WR-1-1. Between 8350 and 7200 cal yr BP, CaO typically varies 12 – 15%, with particularly strong enrichment between 7200 and 6500 cal yr BP. From ~6400 cal yr BP, CaO concentrations decrease sharply but remain elevated (5 – 15%) until ~4600 cal yr BP. Sediments from ~4600 cal yr BP to present generally contained relatively little CaO (< 5%). Variations in S show two major peaks in concentration (15 – 25%) at 8000– 7230 cal yr BP and 6320 – 4770 cal yr BP. A marked decrease in %S is observed from 4770 cal yr BP, with recent sediments containing very low S concentrations (< 1%).

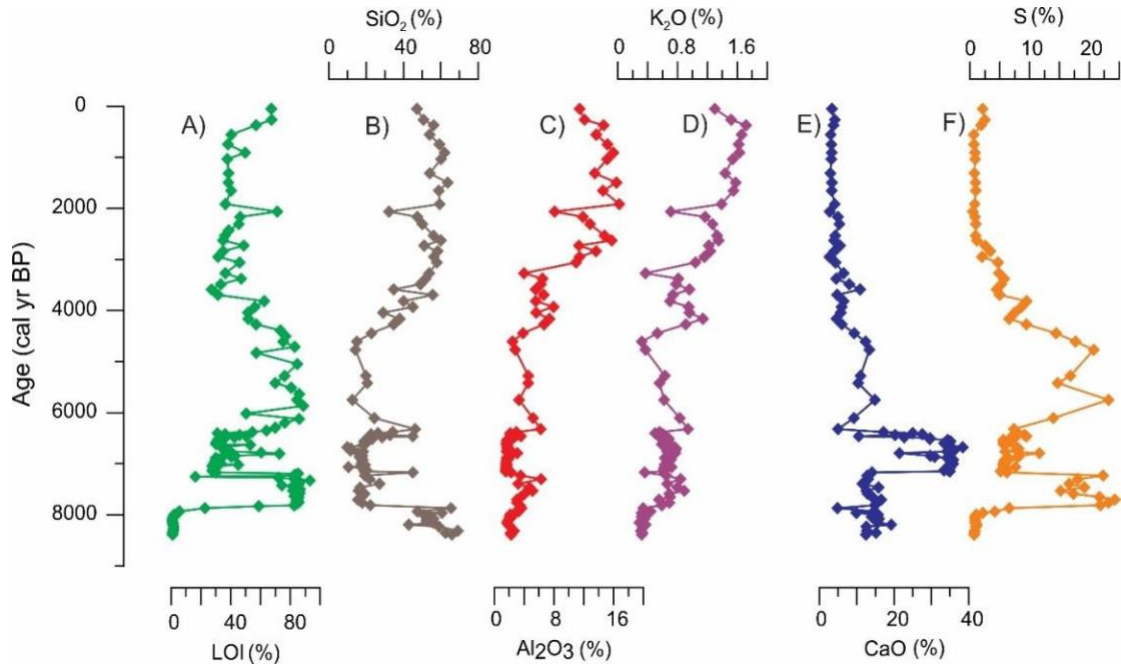


Figure 5.3 Downcore variations in LOI, SiO₂, Al₂O₃, K₂O, CaO and S through core WR-1-1. All XRF data are provided in Appendix 1.

Variations in %TiO₂ (Fig. 5.4A) and %KO₂ (Fig. 5.4B) both show good correlation ($R^2 > 0.8$) with %Al₂O₃. This is an indication of their association mainly with detrital clay minerals.

Variations observed in these elements are thus controlled by silicate sources and reflect the deposition of minerogenic material. In contrast, CaO is not correlated with Al₂O₃ (Fig. 5.4C). In general, sediments with high CaO have corresponding low %Al₂O₃. This indicates that the majority of CaO present in sediments does not form part of the mineralogical fraction and is likely derived from another source. A plot of CaO vs S reveals two distinct groupings; the first characterised by moderate S and high CaO concentrations, the second by moderate CaO and a high S concentrations (Fig. 5.4D).

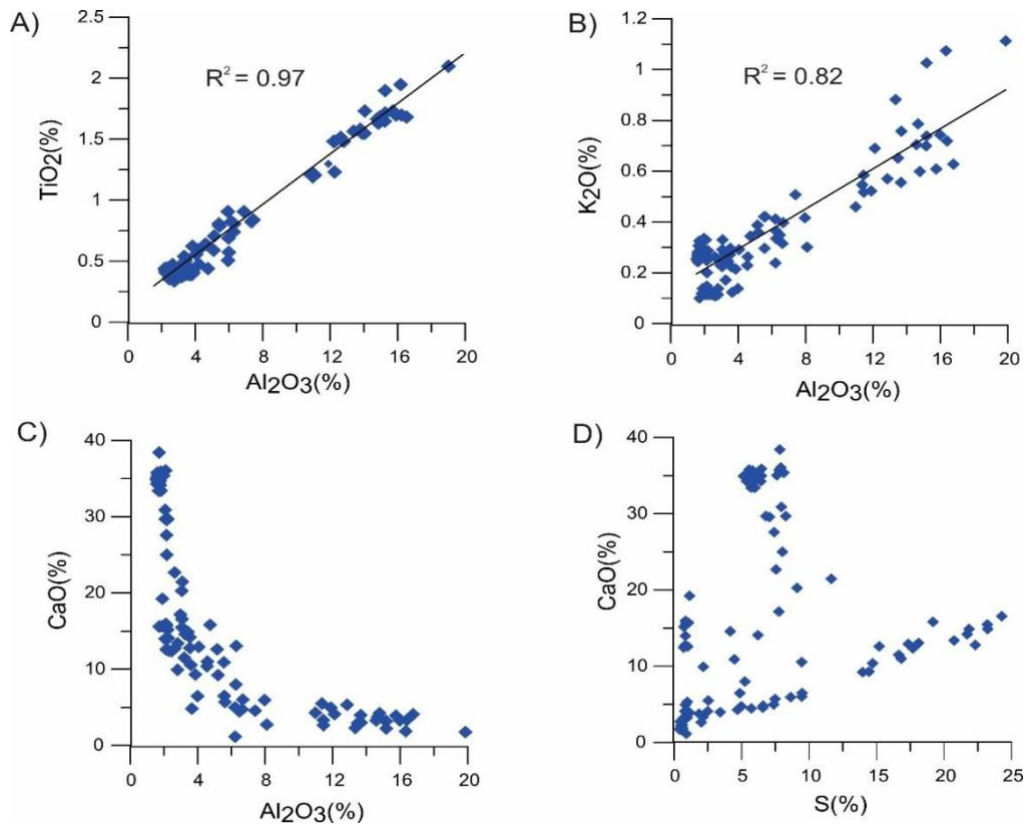


Figure 5.4 Relationship between selected major chemical components of sediments from WR1-1

5.3. Mineralogy

X-ray diffraction analysis reveals that calcite (CaCO_3) and gypsum (CaSO_4) constitute major components of the inorganic fraction (Fig. 5.5). Analysis of samples from 219 – 225 cm (~7400 cal yr BP) and 161 – 165 cm (~6800 cal yr BP) reveal that strong enrichments in S are associated with the presence of gypsum (Fig. 5.5A), while strong enrichments in CaO are associated predominately calcite and lesser amounts of gypsum (Fig. 5.5B).

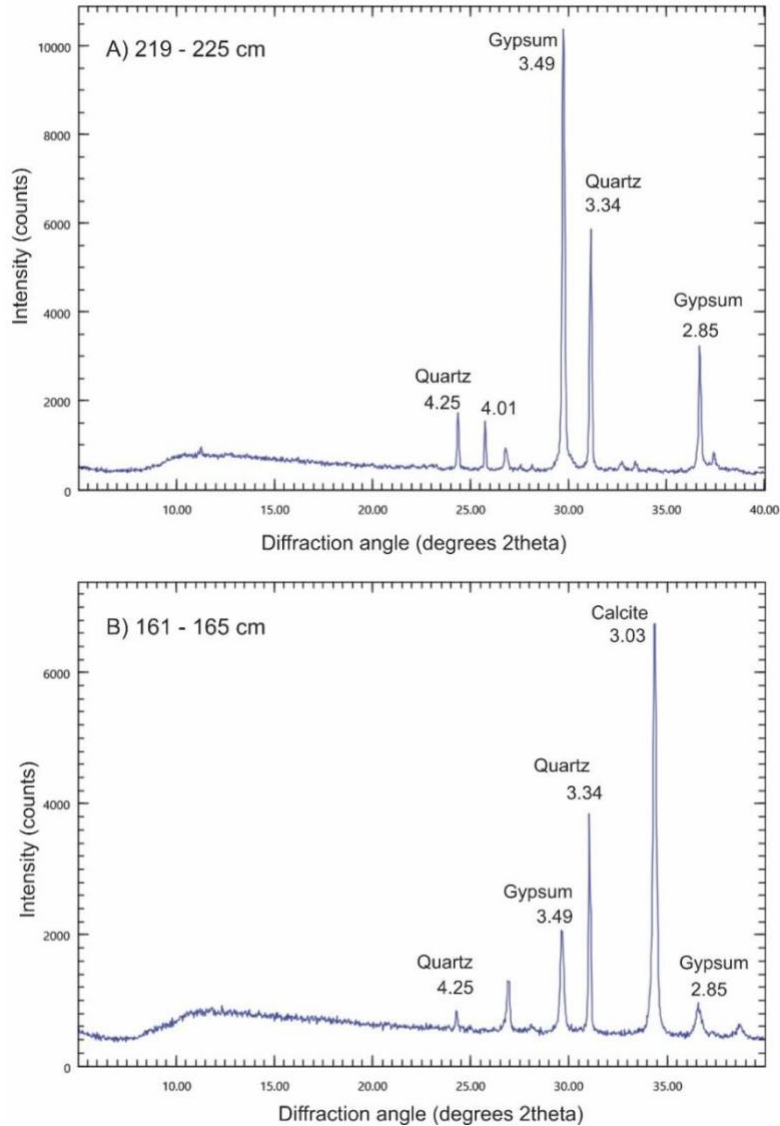


Figure 5.5 X-ray diffraction (XRD) patterns and identified mineral phases for two samples: A) 219 – 225 cm (~7400 cal yr BP) and B) 161 – 165 cm (~6800 cal yr BP).

5.4. Chemical ratios

Ratios of $\text{SiO}_2/\text{Al}_2\text{O}_3$ and $\text{Zr}/\text{Al}_2\text{O}_3$ reveal similar downcore trends (Fig. 5.6). Highest levels of enrichment are found at the bottom of the core between 8500 and 8000 cal yr BP. A sharp decrease in the ratios is observed from 8000 cal yr BP, followed by an increase between 7250 and 6400 cal yr BP. Thereafter, $\text{SiO}_2/\text{Al}_2\text{O}_3$ and $\text{Zr}/\text{Al}_2\text{O}_3$ ratios remain relatively low, apart from a distinct increase between ~3800 and 3200 cal yr BP.

Normalised CaO and Sr concentrations reveal broadly similar downcore trends that initially match those of SiO₂ and Zr (Fig 5.6). Enrichments near the base of the core are followed by a steady decrease between 8000 and 7250 cal yr BP. A period of significant CaO and Sr enrichment is observed between 7250 and 6400 cal yr BP. A sharp decrease in CaO/Al₂O₃ and Sr/Al₂O₃ ratios from 6400 cal yr BP is followed by a more muted, but prolonged, period of enrichment between 6300 and 4200 cal yr BP. This period of enrichment is strongly reflected in S/Al₂O₃ ratios, which show two well-defined peaks centred at 5750 and 4600 cal yr BP (Fig. 5.6). From 4200 cal yr BP, S/Al₂O₃ ratios decline sharply and remain relatively low to present.

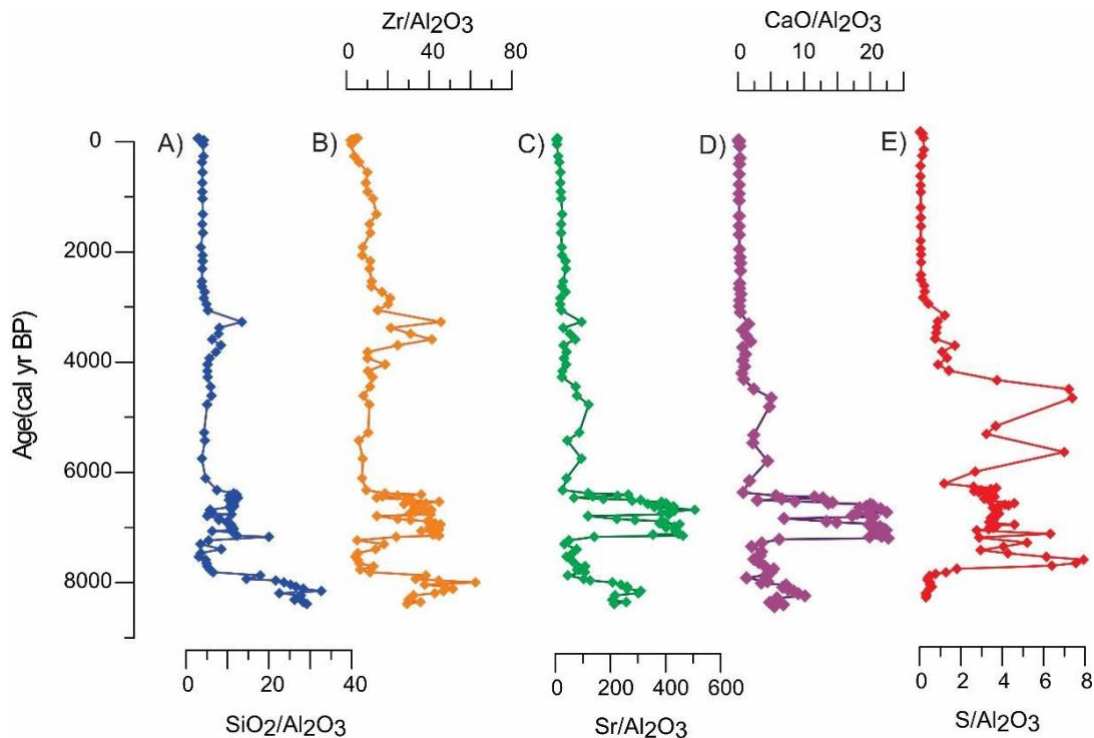


Figure 5.6 Variation in chemical ratio indicators through core WR1-1

5.5. Stable isotope chemistry

Core WR-1-1 is characterised by considerable variations in C_{org}/N, δ¹³C and δ¹⁵N (Fig. 5.7). The C_{org}/N ratio fluctuates between 13.8 and 35.2. A general decline in C_{org}/N values is observed between 8000 and 6700 cal yr BP. A sharp increase is observed at ~6400 cal yr BP, followed by

a gradual decline to ~3000 cal yr BP. The period 2800 – 1900 cal yr BP is characterised by elevated C_{org}/N , with values thereafter remaining fairly constant to present.

The $\delta^{13}C$ signal fluctuates between -29‰ and -19‰ (Fig. 5.7B). The downcore profile is characterised by a pronounced shift in $\delta^{13}C$ to significantly higher values (-19.5‰) between 7300 and 6500 cal yr BP. Thereafter, $\delta^{13}C$ values show a gradual increase from -28.1‰ at 6500 cal yr BP to -21.7‰ at 1500 cal yr BP. The last ~750 years is characterised by a gradual shift to lower $\delta^{13}C$ signatures. The $\delta^{15}N$ signal fluctuates between 2.4‰ and -1.6‰ (Fig. 5.7C). Broadly, an overall shift to lower $\delta^{15}N$ values is observed from 8000 to 5400 cal yr BP. From ~4800 cal yr BP to present, this trend is reversed with a gradual shift to higher $\delta^{15}N$ signatures.

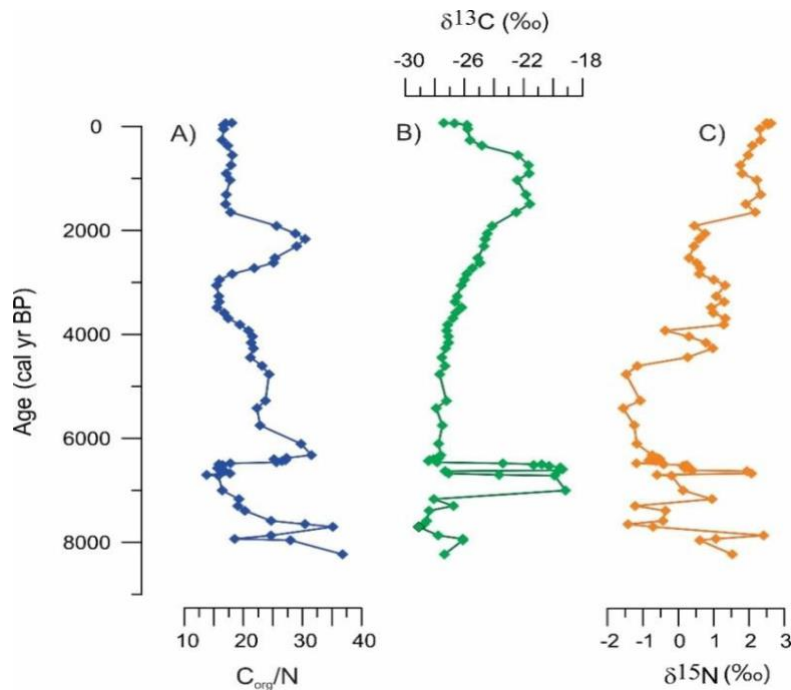


Figure 5.7 Downcore variation in C_{org}/N , $\delta^{13}C$ (‰) and $\delta^{15}N$ (‰) through core WR1-1.

Chapter 6: Discussion

6.1 Introduction

The nature of sedimentary infill at Whale Rock wetland is influenced by the interaction between changes in sediment supply related to relative sea level and climate. Geochemical analysis of WR1-1 reveals the accumulation of sediments of different origin which reflect variations in depositional processes at Whale Rock through time. In this chapter, several geochemical proxies are used to provide insight into the processes that have contributed to the geomorphological evolution of Whale Rock wetland and what this means for paleoenvironmental change along the southern Cape coast more broadly.

6.2 Proxy interpretation

6.2.1 Sea level change and the evolution of Whale Rock wetland

The presence of calcium carbonate and gypsum in coastal sediments can be strong indicators for marine intrusions associated with changes in sea level (Riley and Chester, 2013; Schoepfer, 2013; Wündsche et al., 2016, 2018). At Whale Rock, enrichment in calcium (i.e. $\text{Ca}/\text{Al}_2\text{O}_3$) is associated predominantly with the precipitation of calcium carbonate and gypsum, and can therefore be used to infer changes in the influence of sea level at the site. A marked increase in $\text{Ca}/\text{Al}_2\text{O}_3$ between ~7300 and ~6400 cal yr BP is consistent with a dramatic rise in sea level, reaching present day levels by ~7500 cal yr BP (Fig. 6.1). Along the southern Cape coast, two mid-Holocene sea level highstands at 7000 cal yr BP (+2.5 m) and 6500 cal yr BP (+3.0 m) (Cooper et al., 2018) are strongly reflected by corresponding enrichments in $\text{Ca}/\text{Al}_2\text{O}_3$ at Whale Rock. A sharp decline in $\text{Ca}/\text{Al}_2\text{O}_3$ from ~6400 cal yr BP suggests that marine influence at the site decreased dramatically around this time. This was likely associated with sediment deposition and dune accretion, which served to reduce tidal influence at the site. This is supported by concomitant declines in both $\text{Sr}/\text{Al}_2\text{O}_3$ and $\text{SiO}_2/\text{Al}_2\text{O}_3$ (Fig. 5.6), as well as a shift in diatom assemblages from marine-brackish to freshwater-dominated taxa (Sepato, 2023).

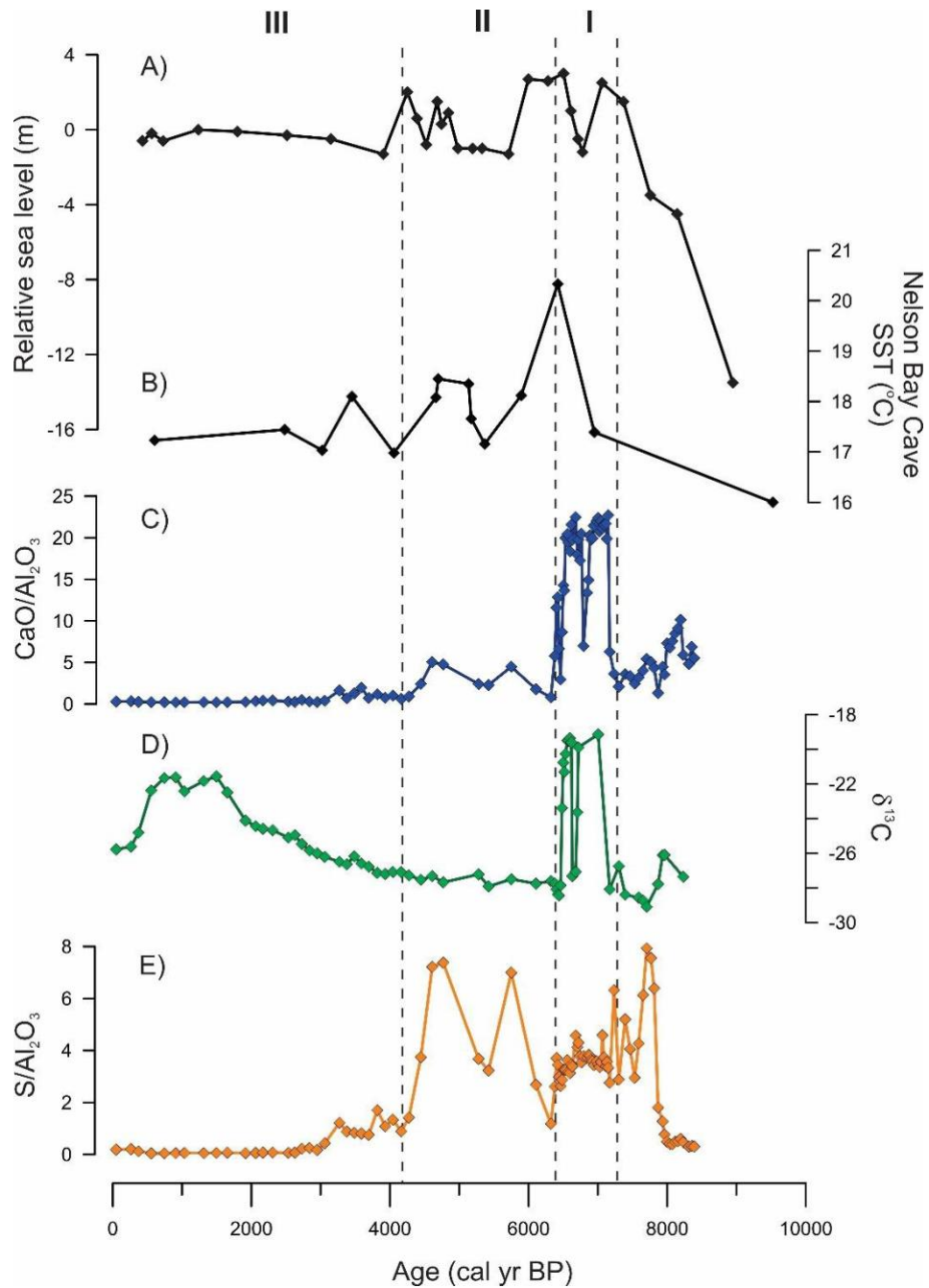


Figure 6.1 Comparison between marine influence geochemical indicators at Whale Rock (WR-1-1) with reconstructed variations in sea level along the southern Cape coast (Cooper et al., 2018) and sea surface temperatures (SST) from Nelson Bay Cave (Cohen and Tyson, 1995). Dashed vertical lines delineate inferred stages in the geomorphological evolution of Whale Rock wetland.

Evidence for changes in marine influence is also reflected in the organic chemistry data. A pronounced shift to higher $\delta^{13}\text{C}$ values is observed between ~ 7300 and ~ 6500 cal yr BP, which corresponds with enrichments in $\text{Ca}/\text{Al}_2\text{O}_3$ (Fig. 6.1) A plot of $\text{C}_{\text{org}}/\text{N}$ vs $\delta^{13}\text{C}$ indicates that organic matter at Whale Rock is derived primarily from C_3 terrestrial plants (Fig. 6.2). Values of $\text{C}_{\text{org}}/\text{N}$ range between 13 and 45, and are typical of C_3 fynbos vegetation that occurs within the region (Quick et al., 2013). However, samples from 7300 – 6500 cal yr BP are characterised by markedly more enriched $\delta^{13}\text{C}$ signatures (-23 to -19‰). This shift in $\delta^{13}\text{C}$ signature suggests mixing between different sources of organic matter and likely reflects the influence of dissolved organic carbon from a marine source.

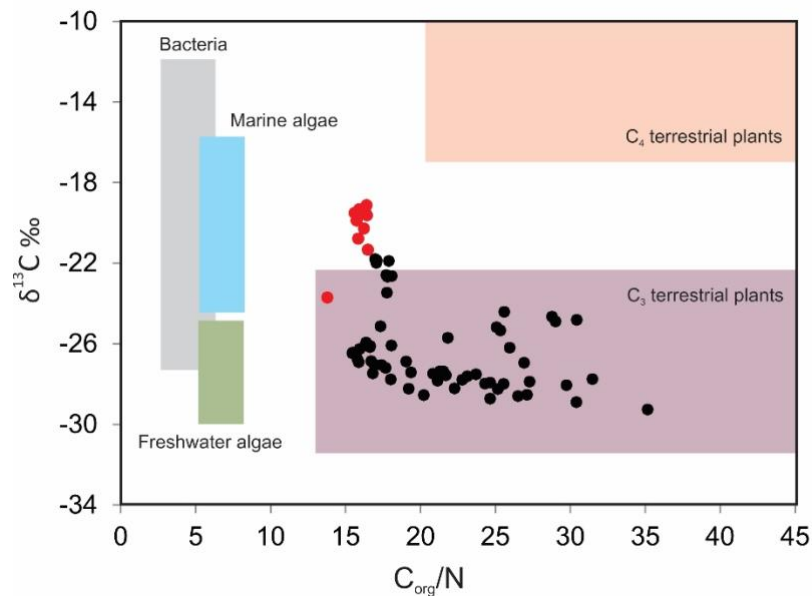


Figure 6.2 Plot of $\delta^{13}\text{C}$ (‰) against $\text{C}_{\text{org}}/\text{N}$ ratio for WR1-1 core samples. Standard ranges for organic inputs to coastal environments are indicated according to Meyers (1994). Samples associated with the sea level highstand shown in red.

While a decline in $\text{Ca}/\text{Al}_2\text{O}_3$ enrichment and a shift to more depleted $\delta^{13}\text{C}$ signatures indicates a significant decrease in marine influence from 6300 cal yr BP, $\text{S}/\text{Al}_2\text{O}_3$ values remain elevated until ~ 4200 cal yr BP. X-ray diffraction analysis revealed that sulfur was present primarily in the form of gypsum, which is likely to have been precipitated from sea water. This suggests that while Whale Rock wetland had largely separated from the ocean by 6300 cal yr BP, it likely continued to receive marine inputs, possibly in the form of occasional barrier overwash, until

~4200 cal yr BP. At this time, the wetland transitioned to a freshwater system and began to accumulate predominantly terrestrially-derived sediments.

6.2.2 Aeolian flux and aridity

Zirconium (Zr) and silicon (Si) are elements typically associated with coarser sediments, and thus enrichment geochemical proxies together with increased grain size indicate increased depositional energy (Kylander et al., 2020; Humphries et al., 2020). Variations in these parameters through WR-1-1 show similar trends and are interpreted to reflect changes in sediment grain size associated with different depositional processes (Fig. 6.3). Enrichment in $\text{SiO}_2/\text{Al}_2\text{O}_3$ and $\text{Zr}/\text{Al}_2\text{O}_3$ between 8350 and 6400 cal yr BP corresponds with a period of significant marine influence (see Fig. 6.1) and therefore reflects increased depositional energy associated with tidal currents. A sharp decline in these ratios signifies a transition to a more tranquil, back-barrier environment from ~6400 cal yr BP. This shift in depositional energy is reflected in a marked decrease in sedimentation rate (see Fig. 5.2). The formation of a more sheltered back-barrier environment promoted the accumulation of terrestrially-derived fine-grained material, particularly from ~4500 cal yr BP, as indicated by the increasing proportion of Al_2O_3 within sediments (Fig. 6.3D).

Tranquil depositional conditions are interrupted by a distinct period of enrichment in $\text{SiO}_2/\text{Al}_2\text{O}_3$ and $\text{Zr}/\text{Al}_2\text{O}_3$ ratios between 3800 and 3200 cal yr BP. Given the hydrological and geomorphological setting of the wetland, deflation from the adjacent coastal dunes represents the most likely source of this material. This suggests that the period 3800 – 3200 cal yr BP may have been characterised by increased wind intensity and/or increased aridity, with reduced dune vegetation cover promoting the aeolian transport of material. Available macrocharcoal data from WR1-1 suggests that charcoal concentrations peaked around 3800 cal yr BP (Ntsondwa, 2021), coinciding with the inferred increase in aeolian-derived material. This suggests that conditions at Whale Rock may have been characterised by increased aridity 3800 – 3200 cal yr BP. It is also possible that enhanced aeolian transport during this period may have been driven by a change in the prevailing wind direction and associated increase in sediment supply.

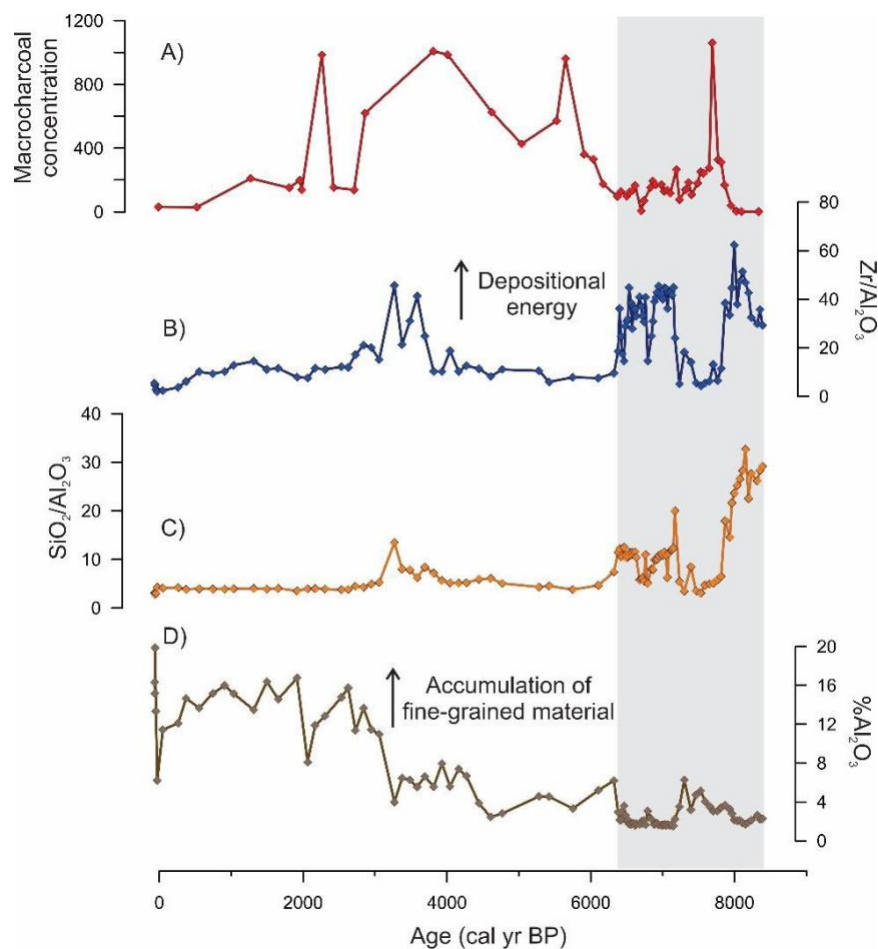


Figure 6.3 Comparison between key environmental proxies at Whale Rock. Macrocharcoal concentrations from Ntsondwa (2021). Grey shading indicates period of the record dominated by marine influence.

6.3 Regional palaeoenvironmental comparison

Recent palaeoenvironmental reconstructions from Eilandvlei and Voëlvlei provide data for the YRZ against which results from Whale Rock can be compared. Wüdsch et al. (2018) used geochemistry and micropalaeontological data to assess changes in marine influence at Eilandvlei, while a marine intrusion at Voëlvlei was inferred from changes in Na concentrations (Strobel et al., 2021). A comparison of marine proxy results from Whale Rock with these two sites reveals a temporally coherent picture (Fig. 6.4). All three records indicate that marine conditions prevailed prior to ~6400 cal yr BP, coincident with a sea level highstand during the early Holocene. A

subsequent abrupt decline in marine indicators from ~6400 cal yr BP is associated with stabilisation in sea level and signifies the point at which the coastal lakes and wetlands along the southern Cape coast started to form and separate from the ocean. The records from Eilandvlei and Voëlvlei suggest that coastal systems did not become entirely hydrologically disconnected from the ocean at this time, with marine influences persisting until ~4000 cal yr BP. This is consistent with the geochemical record from Whale Rock, as revealed by the precipitation of gypsum until ~4200 cal yr BP, and is likely associated with moderate (± 1 m) fluctuations in sea level that occurred over this period (see Fig. 6.1).

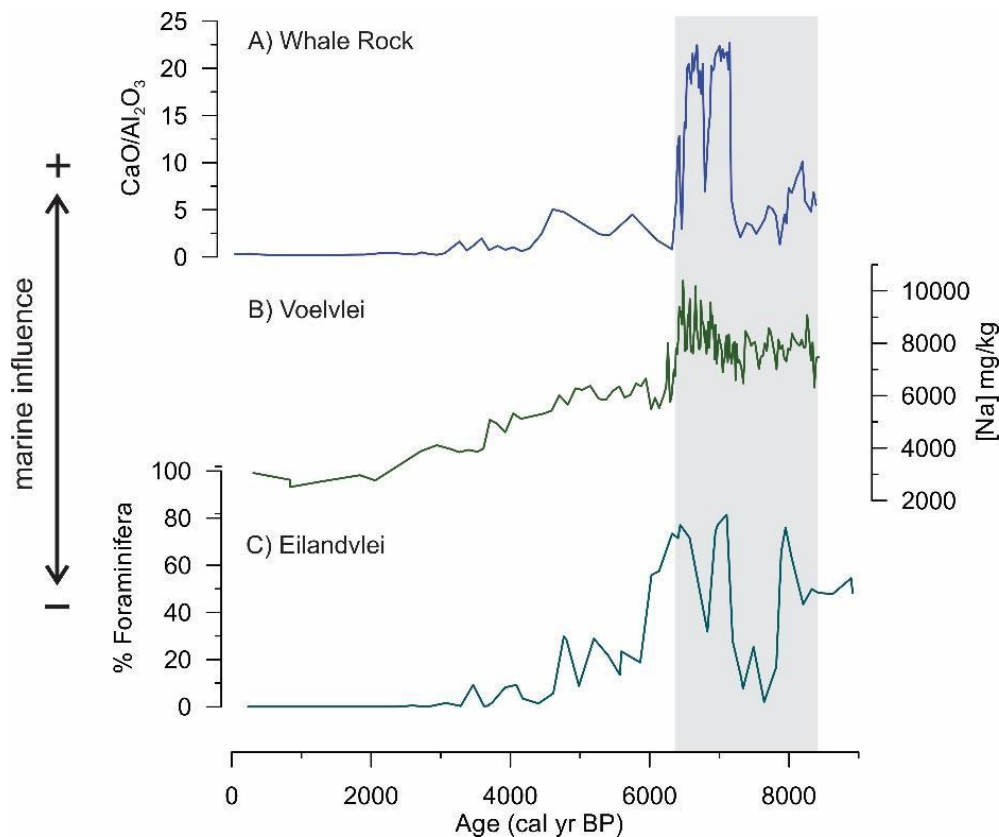


Figure 6.4 Comparison of marine influence proxies from A) Whale Rock wetland (this study), B) Voëlvlei (Strobel et al., 2021), and C) Eilandvlei (Wüdsch et al., 2018). Grey shading indicates period dominated by marine influence.

The geochemical record ($\text{SiO}_2/\text{Al}_2\text{O}_3$ and $\text{Zr}/\text{Al}_2\text{O}_3$) from Whale Rock suggests that the period 3800 – 3200 cal yr BP may have been characterised by increased wind intensity and/or increased aridity. This is generally supported by macrocharcoal data from the site, which suggests an increase in the frequency of fires around this time (Ntsondwa, 2021). At Eilandvlei, a decrease in afrotemperate forest pollen abundance suggests that relatively arid conditions prevailed 4700 to 3500 cal yr BP (Fig. 6.5B) (Quick et al. 2018). This is supported by increasing Al/Si values over this period, which is interpreted to reflect enhanced aeolian flux (Wündsche et al., 2018). At Voëlvlei, an abrupt shift in $\delta^{13}\text{C}_{\text{n-alkane}}$ between 4050 and 3100 cal yr BP is interpreted to reflect a shift towards more arid conditions (Strobel et al., 2021; Fig. 6.5C). The timing of this shift compares well with inferred increases in aridity at Whale Rock from 3800 – 3200 cal yr BP.

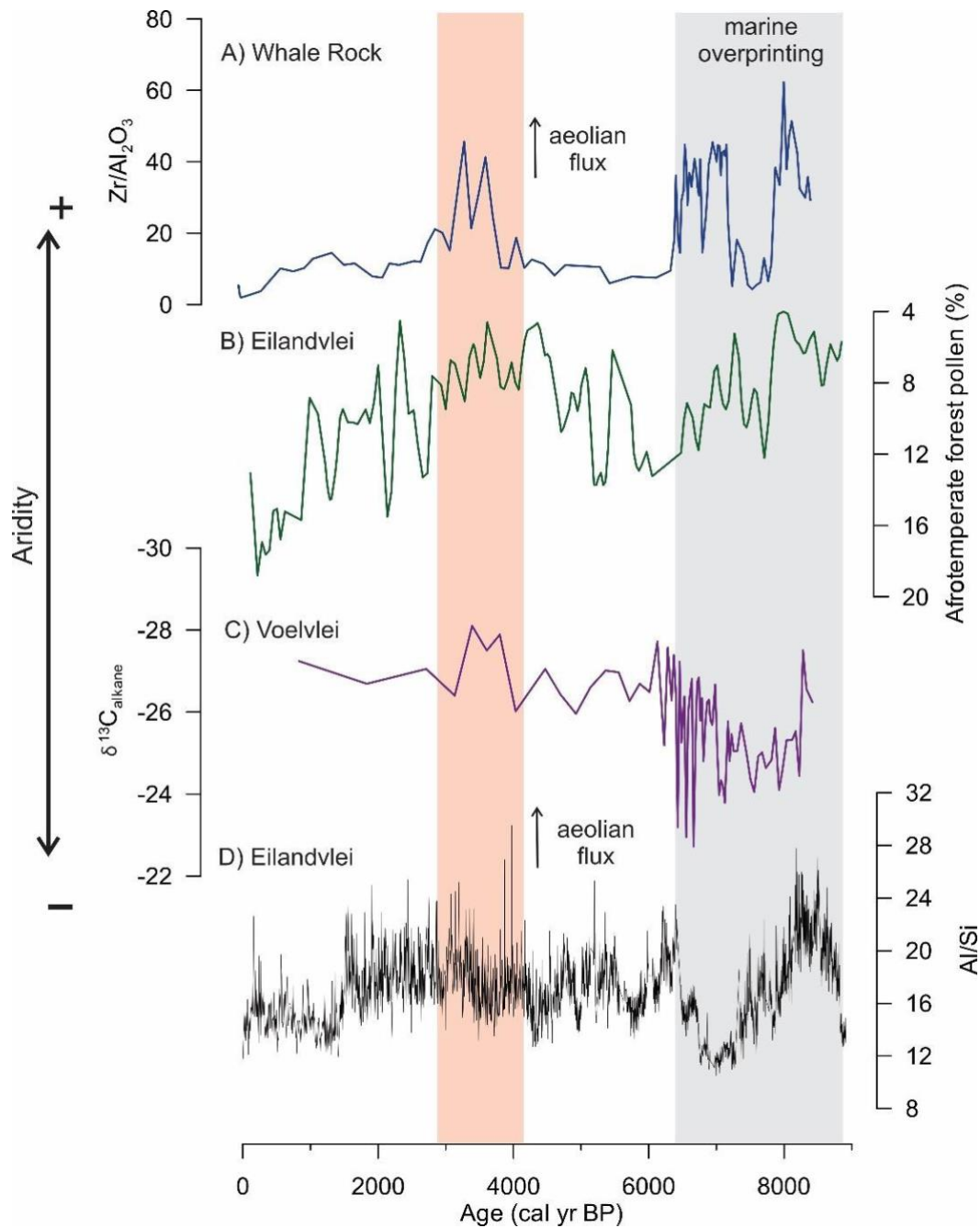


Figure 6.5 Comparison of aridity proxies from A) Whale Rock wetland (this study), B) Eilandvlei (Wüdsch et al., 2018) C) Voelvlei (Strobel et al., 2021), and D) Eilandvlei (Wüdsch et al., 2018). Grey shading indicates period dominated by marine influence.

6.4 Climatic drivers

The climate dynamics of the YRZ are complex with influences from both the westerlies and easterlies. Coastal areas are also influenced by oceanic drivers, such as the Agulhas Current (Chase and Quick 2018). Due to this, the coastal southern Cape subregion (including the Whale Rock, Eilandvlei, Voelvlei records) responds differently to the inland subregion (i.e. the Seweweekspoort record; Chase et al. 2013, 2017) and differently to coastal sites in the WRZ.

The strong marine signals which characterise the bottom of WR1-1 limit the interpretation of any palaeoclimate signals over the early Holocene. However, WR1-1 appears to reveal major environmental changes over the mid to late Holocene, likely driven by changes in both temperature and humidity. The geochemical record from Whale Rock and proxy records from other coastal YRZ sites indicate that the period between ~4000 and 3000 cal yr BP was arid. A possible mechanism for this could be related to a latitudinal shift in the westerly winds.

Reconstructions suggest that sea ice in the Southern Ocean declined dramatically across the 4000 – 3000 cal yr BP period from a Holocene maximum at ~4300 cal yr BP (Fig. 6.6B; Nielsen et al., 2004). It is likely the westerlies may have shifted to a more poleward position during this period, resulting in less winter rainfall (less frequent and/or less intense cold fronts) over the YRZ. Isotope records from Cango Caves suggest that regional SSTs were relatively cool over this period (Fig. 6.6BC, which may have served to further reduce moisture availability).

Another possibility is that the YRZ experienced lower rainfall over this period as a result of reduced subtropical easterly flow. Several records from the east coast of South Africa provide evidence for a major period of aridity ~2600 – 3800 cal yr BP (e.g., Humphries et al., 2019; Miller et al., 2020; Humphries et al., 2020). Elemental data from Lake Muzi in northern KwaZulu-Natal (Fig. 6.6 D) and a δD_{wax} record from the Limpopo River Delta (Fig. 6.6E) both point to the onset of more arid conditions in the coastal regions of the SRZ. This was most likely associated with a reduction in the transport of moisture from the Indian Ocean across the southeastern parts of South Africa. A weakening of this system would have resulted in reduced summer rainfall at Whale Rock.

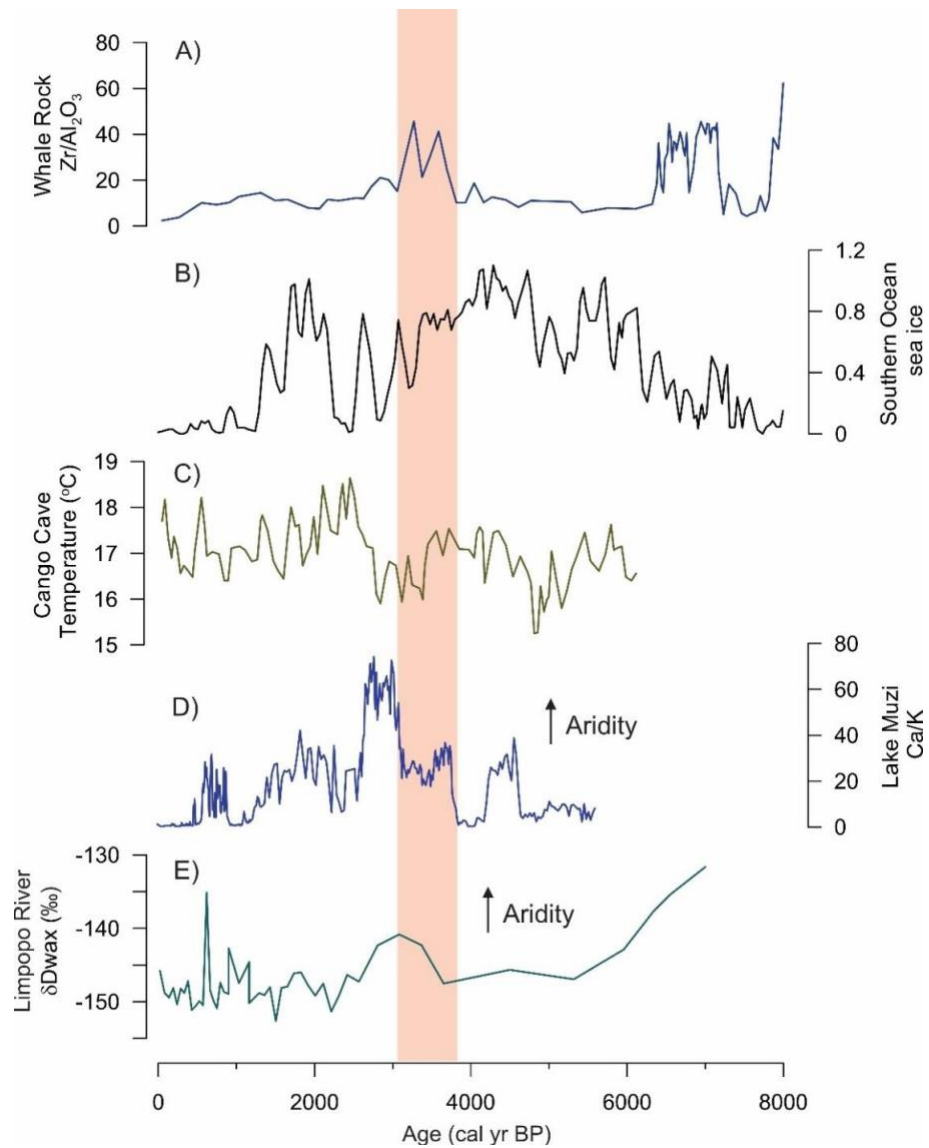


Figure 6.6 Comparison of aridity indicator data (Zr/Al_2O_3) from Whale Rock (A) with other palaeoclimate proxy records. B) Sea ice presence in the Southern Ocean (Nielsen et al., 2004), C) $\delta^{18}O$ temperature reconstruction from Cango Caves (Talma and Vogel, 1992), D) Elemental Ca/K record from Lake Muzi (Humphries et al., 2019), E) δD_{wax} record from the Limpopo River delta (Miller et al., 2020).

Chapter 7: Conclusions

This study used a combination of inorganic elemental and stable isotope geochemical indicators to provide insight into the palaeoenvironmental changes that have occurred at Whale Rock wetland over the Holocene. Enrichments in $\text{Ca}/\text{Al}_2\text{O}_3$ and $\text{S}/\text{Al}_2\text{O}_3$ as well as $\delta^{13}\text{C}$ signatures provide strong indicators of marine influence at the site which prevailed between 8350 and 6400 cal yr BP. Marine influence at the site declined sharply from ~6400 cal yr BP, likely associated with sediment deposition and dune accretion, which served to reduce tidal influence at the site. Enrichments in $\text{SiO}_2/\text{Al}_2\text{O}_3$ and $\text{Zr}/\text{Al}_2\text{O}_3$ provide indicators for depositional energy and suggest that the site transitioned to a sheltered back-barrier environment from ~6400 cal yr. This promoted the accumulation of dominantly terrestrially- derived fine-grained material, particularly from ~4500 cal yr BP. Tranquil depositional conditions are interrupted by a distinct period of enrichment in $\text{SiO}_2/\text{Al}_2\text{O}_3$ and $\text{Zr}/\text{Al}_2\text{O}_3$ ratios between 3800 and 3200 cal yr BP, which is interpreted to reflect enhanced aeolian influx under more arid climate conditions. Recent palaeoenvironmental data from Eilandvlei and Voëlvlei support such an interpretation and suggest that a shift to more arid conditions during this time was likely a broad feature of the climate in the coastal YRZ. The timing of this event corresponds with a marked decrease in Antarctic sea ice and pronounced aridity along the east coast of South Africa, suggesting that mid to late Holocene aridity in the YRZ was likely driven by declines in moisture from both westerly and easterly wind systems.

The geochemical record from Whale Rock provides supporting evidence for understanding the dynamic interactions of temperate and subtropical climate systems on the hydroclimate of the YRZ over the mid to late Holocene. Other sedimentary proxies (e.g., pollen, phytoliths, biomarkers) could potentially be used to extract additional palaeoenvironmental information to corroborate the interpretations presented in this study.

References

- Blaauw, M. and Christen, J. A., 2011. Flexible paleoclimate age-depth models using an autoregressive gamma process. *Bayesian Analysis* 6, 457-474.
- Carr A.S., Bateman, M.D., Cawthra, H.C., Sealy, J., 2019. First evidence for onshore marine isotope stage 3 aeolianite formation on the southern Cape coastline of South Africa. *Marine Geology* 407, 1–15.
- Cartigny, P., Busigny, V., 2018. Nitrogen Isotopes. Springer International Publishing AG, W.G.White (ed.) *Encyclopaedia of Geochemistry*, 1-13. doi: 10.1007/978-3-319-39193-9_197-1.
- Cawthra, H.C., Compton, J.S., Fisher, E.C., MacHutchon, M.R., Marean, C.W., 2015. Submerged shorelines and landscape features offshore of Mossel Bay, South Africa. *Geological Society, London, Special Publications* 411, 219 – 233. doi: 10.1144/SP411.11.
- Cawthra, H.C., Cowling, R.M., Andò, S. and Marean, C.W., 2020. Geological and soil maps of the Palaeo-Agulhas Plain for the Last Glacial Maximum. *Quaternary Science Reviews* 235, p.105858.
- Chase, B.M., Meadows, M.E., 2007. Late Quaternary dynamics of southern Africa’s winter rainfall zone. *Earth-Science Reviews* 84, 103–138. doi: 0.1016/j.earscirev.2007.06.002.
- Chase, B.M., Boom, A., Carr, A.S., 2013. Holocene climate change in southernmost South Africa: rock hyrax middens record shifts in the southern westerlies. *Quaternary Science Reviews* 82, 199–205.
- Chase, B.M., Chevalier, M., Boom, A., 2017. The dynamic relationship between temperate and tropical circulation systems across South Africa since the Last Glacial Maximum. *Quaternary Science Reviews* 174, 54–62.
- Chase, B.M., Faith, J.T., Mackay, A., 2018. Climatic controls on Later Stone Age human adaptation in Africa’s southern Cape. *Journal of Human Evolution* 114, 35–44.
- Chevalier, M., Chase, B.M., 2016. Determining the drivers of long-term aridity variability: A southern African case study. *Journal of Quaternary Science* 31, 143–151. doi: 10.1002/jqs.2850.
- Cohen, A.L., Tyson, P.D., 1995. Sea-surface temperature fluctuations during the Holocene off the south coast of Africa: implications for terrestrial climate and rainfall. *The Holocene* 5, 304–312.

Cohen, J., Zhang, X., Francis, J., 2020. Divergent consensus on Arctic amplification influence on midlatitude severe winter weather. *Nat. Clim. Chang.* 10, 20–29 . <https://doi.org/10.1038/s41558-019-0662-y>.

Compton, J. S., 2001. Holocene sea-level fluctuations inferred from the evolution of depositional environments of the southern Langebaan Lagoon salt marsh, South Africa. *The Holocene* 11, 395–405. <https://doi.org/10.1191/095968301678302832>.

Cooper, J.A.G., Green, A.N., Compton, J.S., 2018. Sea-level change in southern Africa since the Last Glacial Maximum. *Quaternary Science Reviews* 201, 303-318.

Croudace, I.W., Löwemark, L., Tjallingii, T., Zolitschka, B., 2019. Current perspectives on the capabilities of high resolution XRF core scanners. *Quaternary International* 514, 5–15. doi: 10.1016/j.quaint.2019.04.002.

Du Plessis, N., 2020. *Late Holocene environmental and climate dynamics along the southern Cape coast of South Africa: High resolution multi-proxy records from the Wilderness Embayment*. University of Cape Town, PhD Thesis.

Faith, J., Chase, B., & Avery, D., 2019. Late Quaternary micromammals and the precipitation history of the southern Cape, South Africa. *Quaternary Research* 91, 848-860. doi:10.1017/qua.2018.105

Flemming, B., Martin, K., 2021. Sedimentology of a coastal shelf sector characterised by multiple bedload boundaries: Plettenberg Bay, inner Agulhas Bank, South Africa. *Geo-Marine Letters* 32. doi: 10.1007/s00367-021-00702-x.

Francke, A., Holtvoeth, J., Codilean, A.T., Lacey, J.H., Bayon, G., Dossesto, A., 2020. Geochemical methods to infer landscape response to Quaternary climate change and land use in depositional archives: A review. *Earth-Science Reviews*. doi: 10.1016/j.earscirev.2020.103218.

Hahn, A., Compton, J.S., Meyer-Jacob, C., Kirsten, K.L., Lucassen, F., Mayo, M.P., Schefuß, E., Zabel, M., 2016. Holocene paleo-climatic record from the South African Namaqualand mudbelt: A source to sink approach. *Quaternary International* 404, 121–135. doi: 10.1016/j.quaint.2015.10.017.

Hellström, G.B., Lubke, R.A., 1993. Recent changes to a climbing-falling dune system on the Robberg Peninsula, southern Cape coast, South Africa. *J Coast Res* 9, 647–653.

Higgs, C., 2017. *Geochemical insights into the influence of Holocene sea level change on the evolution of the Mkhuze River Delta, Lake St Lucia, northern KwaZulu-Natal*. University of the Witwatersrand, MSc Thesis.

Hogg, A.G., Hua, Q., Blackwell, P.G., Niu, M., Buck, C.E., Guilderson, T.P., Heaton, T.J., Palmer, J.G., Reimer, P.J., Reimer, R.W., 2013. SHCal13 Southern Hemisphere calibration, 0–50,000 years cal BP. *Radiocarbon* 55, 1889-1903.

Humphries, M.S., Kirsten, K.L., McCarthy, T.S., 2019. Rapid changes in the hydroclimate of southeast Africa during the mid- to late-Holocene. *Quaternary Science Reviews* 212, 178-186.

Humphries, M., Green, A., Higgs C., Strachan, K., Hahn, A., Zebel, M., 2020. High-resolution geochemical records of extreme drought in southeastern Africa during the past 7000 years. *Quaternary Science Reviews* 236 (106294). doi: 10.1016/j.quascirev.2020.106294.

Humphries, M., 2021. Elemental proxy evidence for late Quaternary palaeoenvironmental change in southern African sedimentary records: interpretation and applications. *South African Journal of Geology* 124, 1033–1046. doi: 10.25131/sajg.124.0046.

Kirsten, K. L., Haberzettl, T., Wundsch, M., 2018. The impact of sea level changes on the southern Cape coast, South Africa and the variability of the Agulhas Bank environment during the Holocene. *Palaeogeography, Palaeoclimatology, Palaeoecology* 446 (19), 295-207.

Kylander, M.E., Ampel, L., Wohlfarth, B., Veres, D., 2011. High-resolution X-ray fluorescence core scanning analysis of Les Echets (France) sedimentary sequence: new insights from chemical proxies. *Journal of Quaternary Science* 26, 109-117.

Lamb, A.L., Wilson, G.P., Leng, M.J., 2006. A review of coastal palaeoclimate and relative sea-level reconstructions using $\delta^{13}\text{C}$ and C/N ratios in organic material. *Earth-Science Reviews* 75, 29-57.

Mackie, E.A.V., Leng, M.J., Lloyd, J.M., Arrowsmith, C., 2005. Bulk organic $\delta^{13}\text{C}$ and C/N ratios as palaeosalinity indicators within a Scottish isolation basin. *Journal of Quaternary Science* 20, 303-312.

Meyers, P.A., 1994. Preservation of elemental and isotopic source identification of sedimentary organic matter. *Chemical Geology* 114, 289-302.

Meyers, P.A., 1997. Organic geochemical proxies of paleoceanographic, paleolimnological, and paleoclimatic processes. *Org. Geochem* 27, 213–250.

Meyers, P.A., 2003: Applications of organic geochemistry to paleolimnological reconstructions: a summary of examples from the Laurentian Great Lakes. *Organic Geochemistry* 34, 261–289.

Miller, C., Hahn, A., Liebrand, D., Zabel, M., Schefuß, E., 2020. Mid- and low latitude effects on

eastern South African rainfall over the Holocene. *Quaternary Science Reviews* 229, 106088

Mucina, L. Rutherford., M.C., 2006. The vegetation of South Africa, Lesotho and Swaziland. *Strelitzia* 19. *South African National Biodiversity Institute*, Pretoria.

Myers, N., Mittermeier, R.A., Mittermeier, C.G., da Fonseca, G.A.B., Kent, J., 2000. Biodiversity hotspots for conservation priorities. *Nature* 403, 853–858. doi: 10.1038/35002501.

Nangombe, S., Zhou, T., Zhang, W., Wu, B., Hu, S., Zou, L., Li, D., 2018. Recordbreaking climate extremes in Africa under stabilized 1.5 °C and 2 °C global warming scenarios. *Nat. Clim. Change* 8, 375-380.

Naumann, G., Alfieri, L., Wyser, K., Mentaschi, L., Betts, A.R., Carrao, H., Spinoni, J., Vogt, J., Feyen, L., 2018. Global changes in drought conditions under different Levels of warming. *Geophysical Research Papers* 47 (7), 3285-3296. doi: 10.1002/2017GL076521.

Nielsen, S.H.H., Koç, N., Crosta, X., 2004. Holocene climate in the Atlantic sector of the Southern Ocean: controlled by insolation or oceanic circulation? *Geology* 32, 317–320.

Ntsondwa, A., 2021. Reconstructing Holocene fire histories along the southern Cape coast using macrocharcoal from Whale Rock, Plettenberg Bay. Unpublished Honours Thesis. Nelson Mandela University.

Pohl, B., Macron, C., Monerie, P., 2017. Fewer rainy days and more extreme rainfall by the end of the century in Southern Africa. *Sci. Rep.* 7(46466).

Pyke, C.R., Andelman, S.J., Midgley, G., 2005. Identifying priority areas for bioclimatic representation under climate change: a case study for Proteaceae in the Cape Floristic Region, South Africa. *Biological Conservation* 125, 1–9. doi: 10.1016/j.biocon.2004.08.004.

Quick, L.J., 2013. Late Quaternary palaeoenvironments of the southern Cape, South Africa: palynological evidence from three coastal wetlands. University of Cape Town, PhD Thesis.

Quick, L.J., Chase, B.M., Wundsche, M., 2018. A high-resolution record of Holocene climate and vegetation dynamics from the southern Cape coast of South Africa: Pollen and microcharcoal evidence from Eilandvlei. *Journal of Quaternary Science*, 33, 487–500.

Quick, L.J., Chase, B.M., Carr, A.S., Chevalier, M., Grobler, A.B., Meadows, E.M., 2021. A 25,000 year record of climate and vegetation change from the southwestern Cape coast, South Africa. *Quaternary Research* 105, 1-18. doi: 10.1017/qua.2021.3.

Ramsay, P.J., 1995. 9000 Years of sea-level change along the Southern African coastline. *Quaternary International* 31, 71-75.

Ramsay, P., Cooper, A., 2002. Late Quaternary Sea-Level Change in South Africa. *Quaternary Research* 57, 82-90. doi:10.1006/qres.2001.2290.

Riley, J.P., Chester, R., 2013. *Chemical Oceanography*. Academic Press, volume 8.

Rudner, J., Rudner I., 2015. A note on early excavations at Robberg. *The South African Archaeological Bulletin* 28, 94-96.

Schoepfer, V. A., 2013. The influence of sea-water inundation on coupled iron and sulfur cycling in a coastal freshwater wetland. MS thesis, University of Nebraska-Lincoln.

Schropp, S.J., Graham Lewis, F., Windom, H.L., Ryan, J.D., Calder, F.D., Burney, L.C., 1990. Interpretation of metal concentrations in estuarine sediments of Florida using aluminum as a reference element. *Estuaries* 13, 227-235.

Schumann, E.H., Flemming, B.W., Swart, V.P., Hunter, I.T., 1982. Agulhas Bank Studies Report No. 8: report on measurement programmes 20 January to 22 March 1982. NRIO (CSIR) Memorandum 8, 39.

Sepato, T., 2023. Assessing diatom community composition and structure of palaeosediments of a southern Cape coast wetland. Unpublished MSc dissertation. Nelson Mandela University.

Stock, W., Chuba, D., Verboom, G., 2004. Distribution of South African C3 and C4 species of Cyperaceae in relation to climate and phylogeny. *Austral Ecology* 29, 313-319.

Strobel, P., Bliedtner, M., Carr, A. S., Frenzel, P., Klaes, B., Salazar, G., Struck, J., Szidat, S., Zech, R., and Haberzettl, T., 2021. Holocene sea level and environmental change at the southern Cape – an 8.5 kyr multi-proxy paleoclimate record from Lake Voëlvlei, South Africa, *Climate Past* 17, 1567–1586. doi:10.5194/cp-17-1567-2021.

Talma, A.S., Vogel, J.C., 1992. Late Quaternary paleotemperatures derived from a Speleothem from Cango Caves, Cape Province, South Africa. *Quaternary Research* 37, 203–213.

Tyson, P.D., Preston-Whyte, R.A., 2000. *The Weather and Climate of Southern Africa*. Oxford University Press, Cape Town.

Vogel, J.C., Fuls, A., Ellis, R.P., 1978. The geographical distribution of Kranz grasses in South Africa. *S. Afr. J. Sci.* 74, 209–215.

Wada, E., Kadonaga, T., Natsuo, S., 1975. ^{15}N abundance in naturally occurring substances and global assessment of denitrification from isotopic viewpoint. *Geochem journal*, 9, 139–148.

Walker, M., Johnsen, S., Rasmussen, S.O., Steffensen, J., Popp, T., Gibbard, P., Hoek, W., Lowe, J., Andrews, J., Björck, S., Cwynar, L., Hughen, K., Kershaw, P., Kromer, B., Litt, T., Lowe, D.J., Nakagawa, T., Newnham, R.M. & Schwander, J., 2008. The Global Stratotype Section and Point (GSSP) for the base of the Holocene Series / Epoch (Quaternary System / Period) in the NGRIP ice core. *Episodes* 31, 264–267.

Wündsche, M., Haberzettl, T., Kirsten, K.L., Kasper, T., Zabel, M., Dietze, E., Baade, J., Daut, G., Meschner, S., Meadows, M.E., 2016. Sea level and climate change at the southern cape coast, South Africa, during the past 4.2 kyr. *Palaeography Palaeoclimatology Palaeoecology* 446, 295-307.

Wündsche, M., Haberzettl, T., Cawthra, H.C., Kirsten, K.L., Zabel, M., Frenzel, P., Hahn, A., Baade, J., Daut, G., Kasper, T., Meadows, E.M., Mausbacher, R., 2018. Holocene environmental change along the southern Cape coast of South Africa - Insights from the Eilandvlei sediment record spanning the last 8.9 kyr. *Global and Planetary Change* 163, 51-66. <https://doi.org/10.1016/j.gloplacha.2018.02.002>.

Appendix

Table 1 XRF data

Depth (cm)	Age (cal yr BP)	SiO ₂ (%)	Fe ₂ O ₃ (%)	Al ₂ O ₃ (%)	CaO (%)	TiO ₂ (%)	K ₂ O (%)	S (%)	Sr (ppm)	Zr (ppm)	LOI (%)
5,0	-66	50,43	8,5	16,33	1,87	0,93	2,32	0,64	129	88	42,78
9,0	-61	46,8	5,13	15,18	2,22	0,9	2,22	0,52	107	68	32,39
12,0	-58	55,13	4,8	19,87	1,75	1,02	2,4	0,41	131	102	33,90
14,0	-47	40,68	4,31	13,34	2,29	0,71	1,92	0,58	76	38	49,20
17,5	-29	26,61	1,44	6,22	1,14	0,19	0,58	0,90	31	12	63,02
19,0	50	47,19	3,65	11,44	3,33	0,5	1,3	2,12	69	27	67,22
22,0	264	50,72	4,66	12,11	4,11	0,65	1,52	2,49	126	45	67,37
23,5	372	56,14	5,6	14,67	3,76	0,74	1,72	1,85	210	89	57,01
25,5	555	53,98	5,0	13,68	3,01	0,8	1,66	0,62	258	138	40,40
27,5	745	59,22	4,98	15,18	3,18	0,79	1,62	0,68	276	141	38,15
29,5	908	62,01	4,84	15,98	3,28	0,78	1,63	0,84	322	163	49,70
31,0	1034	60,08	5,01	15,15	3,16	0,75	1,54	0,87	326	194	37,80
34,0	1313	54,1	4,55	13,48	2,93	0,69	1,44	0,73	338	195	38,53
36,0	1495	63,69	4,85	16,39	3,33	0,78	1,58	0,91	347	182	38,42
38,0	1653	58,92	5,66	14,58	3,27	0,76	1,55	0,96	312	168	40,30
41,0	1915	59,38	6,22	16,77	4,09	0,77	1,39	0,78	396	132	36,47
43,0	2062	32,18	4,32	8,09	2,73	0,39	0,71	0,47	196	61	71,17
45,0	2167	47,37	8,2	11,89	4,95	0,67	1,17	0,83	443	137	46,33
47,0	2306	50,08	5,46	12,85	5,33	0,7	1,27	0,97	498	142	45,44
51,0	2534	56,1	4,43	14,78	4,23	0,77	1,33	0,94	422	180	38,70
53,0	2627	60,03	3,85	15,75	3,9	0,8	1,35	1,15	370	188	36,11
55,0	2728	51,04	3,96	11,36	5,5	0,65	1,22	2,53	429	195	34,90

57,0	2839	58,24	3,7	13,66	3,98	0,69	1,24	3,41	253	288	48,78
59,0	2949	56,25	3,32	11,45	2,65	0,65	1,16	2,01	197	230	34,91
61,0	3058	57,87	3,73	10,97	4,29	0,54	1,04	4,69	242	166	31,55
65,0	3270	53,77	2,51	3,99	6,47	0,24	0,37	4,86	382	182	45,94
67,0	3376	51,83	6,85	6,47	4,47	0,38	0,81	5,71	186	138	36,33
69,0	3485	49,01	3,2	6,26	7,99	0,3	0,78	5,24	331	194	47,06
71,0	3587	34,75	4,17	5,55	10,9	0,37	0,96	4,47	402	229	33,39
73,0	3693	55,63	3,47	6,63	4,75	0,33	0,74	4,97	196	164	27,12
75,0	3816	39,93	5,89	5,57	6,49	0,36	0,7	9,48	228	57	31,40
77,0	3930	44,98	6,17	7,96	5,94	0,38	0,95	8,64	251	81	62,49
79,0	4042	29,06	7,6	5,61	5,7	0,36	0,96	7,48	222	105	56,19
81,0	4162	37,93	9,39	7,4	4,56	0,43	1,14	6,56	190	76	51,59
83,0	4271	34,67	11,38	6,67	6,01	0,37	0,91	9,45	160	84	51,83
85-87	4444,5	22,82	10,73	3,86	9,31	0,22	0,53	14,44	285	44	57,01
89,0	4608	14,97	8,59	2,45	12,35	0,12	0,32	17,69	193	20	73,26
92,0	4769	14,24	5,86	2,81	13,38	0,13	0,37	20,74	340	31	76,78
101,0	5279	19,78	9,28	4,57	11	0,27	0,63	16,83	397	48	75,21
103,5	5421	20,6	12,66	4,55	10,39	0,27	0,56	14,70	197	27	82,91
109,0	5750,5	12,6	3,14	3,32	14,88	0,12	0,62	23,23	315	26	57,19
115,0	6106,5	24,3	8,52	5,2	9,22	0,31	0,83	13,97	214	39	84,64
120,0	6322	46,23	7,42	6,21	4,99	0,43	0,94	7,38	166	59	76,12
123,5	6379	34,21	4,19	2,97	17,17	0,21	0,56	7,77	352	55	69,82
125,5	6401	26,33	3,29	2,16	25,01	0,13	0,5	8,02	572	78	80,51
127,5	6422	22,55	3,4	2,15	27,59	0,14	0,6	7,41	485	53	85,99
129,0	6438	32,74	4,58	3,05	20,27	0,15	0,62	9,11	415	53	84,45
131,5	6462	44,91	5,9	3,59	10,55	0,26	0,55	9,45	244	52	88,60
133,5	6481	28,51	3,79	2,63	22,69	0,16	0,63	7,55	459	76	50,31
135,5	6501	21,5	2,77	2,08	29,69	0,14	0,68	6,79	644	64	85,96
137,0	6515	23,17	2,8	2,17	29,59	0,14	0,63	7,07	605	69	76,27
139,0	6534	19,75	2,15	1,72	34,36	0,14	0,68	5,59	662	77	69,86

141,5	6560	18,84	2,05	1,72	35,17	0,14	0,66	6,24	691	66	63,95
143,0	6575	20,19	2,06	1,76	34,09	0,13	0,66	5,62	591	49	54,42
145,0	6597	19,87	2,1	1,82	33,42	0,14	0,65	5,70	682	67	31,07
147,0	6617	18,65	2	1,61	34,71	0,13	0,59	5,59	690	58	36,23
148,5	6632	18,41	2,23	1,76	34,71	0,14	0,61	5,96	633	58	45,93
153,0	6678	9,83	2,45	1,71	38,42	0,14	0,76	7,83	865	70	50,31
155,5	6704	11,86	2,96	1,97	35,38	0,14	0,78	8,13	850	73	42,57
157,0	6719	11,22	2,74	1,81	35,71	0,14	0,74	7,78	739	60	36,00
159,0	6741	11,56	3,09	2,09	36,07	0,14	0,77	7,91	806	64	31,72
161,0	6761	18,37	2,19	1,67	34,19	0,13	0,66	5,92	688	68	31,72
164,0	6792	15,68	7,36	3,08	21,46	0,19	0,77	11,64	366	45	32,40
169,0	6845	17,9	3,44	2,22	29,69	0,16	0,68	8,27	496	55	30,46
171,0	6865	16,38	3,25	2,07	30,89	0,15	0,66	7,95	598	64	30,28
173,0	6885	16,86	2,22	1,69	34,26	0,15	0,63	6,42	652	66	30,14
175,0	6903	17,46	2,33	1,77	34,98	0,15	0,66	6,46	705	72	53,10
177,0	6922	18,06	2,23	1,8	35,89	0,14	0,71	6,47	680	77	35,17
179,0	6942	17,78	2,1	1,65	35,38	0,14	0,66	5,69	744	75	33,69
183,0	6983	17,97	2,13	1,62	35,67	0,14	0,67	5,80	700	68	35,90
185,0	7003	17,34	2,12	1,6	35,78	0,13	0,64	5,55	642	64	35,44
187,0	7023	19,32	2,08	1,68	34,86	0,14	0,63	5,66	734	75	36,50
189,0	7045	17,41	2,07	1,6	35,27	0,15	0,65	5,68	701	71	39,83
191,0	7065	10,45	2,6	1,66	35,05	0,13	0,72	7,62	724	60	60,42
193,0	7086	18,29	2,08	1,62	34,93	0,14	0,62	6,05	711	69	72,66
195,5	7113	18,78	1,92	1,58	34,27	0,14	0,62	5,35	707	68	42,86
197,0	7128	20,19	1,98	1,68	33,4	0,13	0,63	5,98	595	70	40,46
199,0	7149	18,97	1,97	1,54	34,94	0,15	0,61	5,14	713	69	30,03
201,0	7170	44,98	1,23	2,25	14,08	0,15	0,36	6,21	318	54	33,32
207,0	7233	19,23	1,05	3,53	12,79	0,12	0,65	22,31	175	18	32,19
214,0	7301	21,76	1,79	6,28	13,05	0,23	0,84	18,11	207	114	29,68
223,0	7392,5	27,13	1,49	3,2	11,5	0,16	0,66	16,64	249	45	33,19

230,0	7464,5	16,72	2,56	4,73	15,82	0,15	0,8	19,18	297	26	28,67
235,0	7529,5	15,82	2,35	5,15	12,61	0,24	0,89	15,19	209	22	45,13
241,0	7589	19,1	1,83	4,06	12,93	0,17	0,69	17,35	235	22	27,57
247,0	7652	17,56	2,66	3,54	14,2	0,14	0,7	21,71	250	22	30,74
252,0	7703,5	15,55	1,15	3,06	16,56	0,12	0,55	24,28	331	40	29,42
258,0	7764,5	17,82	0,81	3,07	15,47	0,13	0,69	23,21	244	20	28,25
263,0	7812	22,2	1,01	3,42	14,88	0,15	0,59	21,85	367	39	27,83
268,5	7869	65,44	0,79	3,65	4,83	0,13	0,34	6,59	165	140	27,90
273,0	7934	47,51	0,72	3,26	14,58	0,14	0,44	4,15	337	109	30,28
275,0	7962	60,62	0,69	2,8	9,92	0,11	0,32	2,16	355	125	85,22
277,0	7996	50,83	0,64	2,15	15,71	0,16	0,39	1,06	446	134	83,69
279,0	8037	52,01	0,61	2,06	13,98	0,1	0,32	0,83	490	78	82,30
281,0	8075	56,04	0,63	2,11	15,94	0,17	0,36	0,84	551	100	16,30
283,0	8112	52,32	0,64	1,85	15,64	0,1	0,33	0,91	483	95	72,17
285,0	8153	55,86	0,57	1,71	15,6	0,13	0,29	0,87	530	80	82,44
287,0	8193	42,83	0,68	1,9	19,23	0,14	0,37	1,14	571	81	93,11
289,0	8232	59,01	0,64	2,13	12,58	0,12	0,33	1,00	462	69	86,23
293,0	8314	69,11	0,62	2,64	12,73	0,11	0,31	0,80	545	79	85,78
295,0	8353	62,55	0,59	2,21	15,18	0,09	0,33	0,73	569	79	85,72
296,5	8388	65,93	0,58	2,26	12,45	0,09	0,32	0,70	484	66	74,38

Table 2 Stable isotope data

Age (cal yr BP)	$\delta^{13}\text{C}$ (‰)	$\delta^{15}\text{N}$ (‰)	C:N ratio
-66	-27,79	2,81	18,04
-58	-27,05	2,94	16,95
-29	-26,19	2,85	16,64
50	-26,14	2,62	16,67
264	-25,97	2,64	16,39
372	-25,15	2,40	17,35
555	-22,66	2,29	18,12
745	-21,92	2,05	17,91
908	-21,88	2,11	17,11
1034	-22,62	2,24	17,74
1313	-22,01	2,35	17,08
1495	-21,82	2,21	16,99
1653	-22,69	2,20	17,83
1915	-24,44	0,73	25,61
2062	-24,68	0,77	28,80
2167	-24,84	0,60	30,45
2306	-24,92	0,44	29,03
2534	-25,36	0,31	25,35
2627	-25,21	0,52	25,10
2728	-25,73	0,64	21,85
2839	-26,11	0,59	18,09
2949	-26,29	1,01	15,96
3058	-26,49	1,34	15,47
3270	-26,78	1,08	15,81
3376	-26,93	1,31	15,90
3485	-26,46	0,94	15,52
3587	-26,89	1,00	16,74
3693	-27,08	1,34	17,41
3816	-27,45	1,30	19,40
3930	-27,51	-0,38	20,86
4042	-27,39	0,30	21,54
4162	-27,40	0,79	21,31
4271	-27,59	0,98	21,72
4444,5	-27,85	0,26	21,18
4608	-27,63	-1,17	23,16
4769	-28,00	-1,50	24,33
5279	-27,53	-1,09	23,74
5421	-28,24	-1,58	22,31

5750,5	-27,81	-1,26	22,82
6106,5	-28,07	-1,19	29,77
6322	-27,77	-0,78	31,51
6379	-27,91	-0,64	27,30
6401	-28,26	-0,56	25,19
6422	-28,55	-0,87	27,13
6438	-28,62	-0,67	26,53
6462	-28,01	-0,52	25,58
6481	-26,96	-0,74	26,95
6501	-23,49	-1,23	17,79
6515	-20,81	-0,45	15,85
6534	-21,36	0,21	16,50
6560	-20,30	0,11	16,25
6575	-19,53	0,22	15,83
6597	-19,52	0,16	15,61
6617	-19,38	0,32	15,94
6632	-19,63	0,37	16,43
6678	-27,48	1,94	16,83
6704	-27,22	2,07	17,71
6719	-23,73	-0,64	13,80
7003	-19,92	-0,23	15,78
7170	-19,16	0,11	16,42
7301	-28,25	0,93	19,25
7392,5	-26,89	-1,27	19,07
7589	-28,57	-0,40	20,25
7652	-28,74	-0,47	24,68
7703,5	-28,92	-1,47	30,43
7869	-29,28	-0,75	35,17
7934	-27,95	2,41	24,68
7962	-26,22	1,55	25,97